New human angiotensin converting enzyme 2 (ACE2) knock-in CD-1 mouse model of asymptomatic SARS-CoV-2 infection

Dhanesh Patel

Department of Human Genetics, Faculty of Medicine and Health Sciences

McGill University, Montreal, Quebec, Canada

July 2022

A thesis submitted to McGill University in partial fulfillment of the requirements of the degree of Master of Science (M.Sc.)

Table of Contents

Abstract

The coronavirus disease 2019 (COVID-19) pandemic caused by severe acute respiratory syndrome coronavirus 2 (SARS-CoV-2) continues to cause unprecedented global economic and health burdens. Humans infected with SARS-CoV-2 have variable disease presentation, from asymptomatic to severe. While a lot of research focuses on the severe and critical forms of disease, less is known about milder forms of disease which compromise almost 90% of infectious cases and can lead to relevant complications including immune alterations at the fetal-maternal interfaces and post-acute sequelae of COVID-19 (PASC). Mouse models are essential for modeling the complex *in vivo* interactions between the many cell types and physiological systems that underlie SARS-CoV-2 pathogenesis and to validate candidate human genes for pre-clinical development of therapeutic interventions. Moreover, mouse models can be developed that vary in early immune responses and have different responses to, and outcomes of, SARS-CoV-2 infection. Here we present a new human angiotensin converting enzyme 2 (*hACE2*) knock-in (KI) model generated in the CD-1 strain. Following intranasal inoculation with SARS-CoV-2, the course of infection in *hACE2* KI mice was compared to the keratin 18 (K18)-*hACE2* transgenic model in the C57BL/6J (B6) strain, a known model of severe SARS-CoV-2 infection. *hACE2* KI mice showed no clinical signs despite substantial virus replication in the lung in contrast to B6 K18-*hACE2* mice that showed severe clinical signs with high lethality. Cytokine profiling and RNA sequencing of infected lung tissues demonstrated divergent early host response signatures revealing the combined effect of virus load, *hACE2* expression & tropism, and mouse genetic backgrounds. Furthermore, in the CD-1 *hACE2* KI compared to the B6

K18-*hACE2* mice, interferon signaling, T cell response initiation, inflammatory responses, and cytokine and chemokine signaling are less induced and/or less activated, mirroring findings in transcriptomic profiling of peripheral blood mononuclear cells (PBMCs) from asymptomatic humans relative to symptomatic and/or moderate/severe cases. This new *hACE2* KI model provides a useful tool to study the determinants of asymptomatic SARS-CoV-2 infection and to evaluate environmental or genetic perturbations that increase disease severity or susceptibility.

Résumé

La pandémie de maladie à coronavirus 19 (COVID-19) causée par le coronavirus 2 du syndrome respiratoire aigu sévère (SRAS-CoV-2) continue de représenter un fardeau économique et sanitaire mondial sans précédent. Les personnes infectées par le SRAS-CoV-2 présentent des symptômes variables, allant d'asymptomatiques à graves. Alors que de nombreuses recherches se concentrent sur les formes graves et critiques de la maladie, on en sait moins sur les formes plus légères de la maladie qui compromettent près de 90 % des cas infectieux et peuvent entraîner des complications pertinentes, notamment des altérations immunitaires aux interfaces fœto-maternelles et des séquelles post-aiguës du COVID-19. Les modèles murins sont essentiels pour modéliser les interactions complexes *in vivo* entre les nombreux types de cellules et systèmes physiologiques qui sous-tendent la pathogenèse du SRAS-CoV-2 et pour valider les gènes humains candidats pour le développement préclinique d'interventions thérapeutiques. De plus, il est possible de développer des modèles de souris dont les réponses immunitaires précoces varient et qui présentent des réponses et des résultats différents à l'infection par le SRAS-CoV-2. Nous présentons ici un nouveau modèle de knock-in (KI) de l'enzyme de conversion de l'angiotensine humaine 2 (*hACE2*) généré dans la variété CD-1. Après inoculation intranasale de SRAS-CoV-2, l'évolution de l'infection chez les souris *hACE2* KI a été comparée au modèle transgénique kératine 18 (K18)-*hACE2* de la variété C57BL/6J (B6), un modèle connu d'infection sévère par SRAS-CoV-2. Les souris *hACE2* KI n'ont présenté aucun signe clinique malgré une réplication importante du virus dans les poumons, contrairement aux souris B6 K18-*hACE2* qui ont présenté des signes cliniques sévères avec une létalité élevée. Le profilage des cytokines

et le séquençage de l'ARN des tissus pulmonaires infectés ont mis en évidence des signatures divergentes de la réponse précoce de l'hôte, révélant l'effet combiné de la charge virale, de l'expression et du tropisme de *hACE2*, et des antécédents génétiques des souris. En outre, chez les souris CD-1 *hACE2* KI par rapport aux souris B6 K18-*hACE2*, la signalisation de l'interféron, l'initiation de la réponse des cellules T, les réponses inflammatoires et la signalisation des cytokines et des chimiokines sont moins induites et/ou moins activées, ce qui reflète les résultats du profilage transcriptomique des cellules mononucléaires du sang périphérique (PBMC) des humains asymptomatiques par rapport aux cas symptomatiques et/ou modérés/sévères. Ce nouveau modèle *hACE2* KI constitue un outil pour étudier les déterminants de l'infection asymptomatique par le SRAS-CoV-2 et pour évaluer les perturbations environnementales ou génétiques qui augmentent la gravité de la maladie ou la sensibilité à celle-ci.

Acknowledgements

“The most important step a man can take. It's not the first one, is it? It's the next one” (Sanderson, 2017). Silvia, my supervisor, was the one holding my hand and guiding me through this journey, step by step. Thank you, Dr. Silvia M. Vidal, for believing in me and allowing me to be a part of your lab. I was given the opportunity to work on a fantastic project that will be a foundational pillar of my learning and growth. You encouraged me for any idea I may have, adding many more to the mix, leading to the concoction of a great project of which I am proud of.

Secondly, thank you to Benoit Charbonneau, Patricia Caroline D’Arcy, and Dr. Mitra Yousefi for helping me with the crucial *in vivo* mouse infection experiments of this project in our very own biosafety level 3 (BSL3) facility (the setting up of which was no small feat!). I would also like to thank Dr. Lauryl Nutter and Dr. Bin Gu from The Center for Phenogenomics (TCP) for letting me use the CD-1 *hACE2* KI mouse model they generated in my thesis. In addition, my supervisory committee members Dr. Judith Mandl, Dr. Danielle Malo, and Dr. Rob Sladek were very kind in providing guidance throughout this project.

“Take what is offered and that must sometimes be enough” (Morgan, 2002). These were my feelings after running most of my R code or genpipes ribonucleic acid (RNA) sequencing (RNA-seq) scripts but with the help of Jesse Islam as well as HanChen Wang and Mathieu Mancini, I was able to squeeze out the most from my data and make sure the analysis was done properly.

Finally, and perhaps most importantly, I would like to thank my lab members Dr. Gaël Galli, Nathan Markarian, Dr. Catalina Barboza-Solis, Anqi Yan, and Alice Hou as

well as peers Dr. Angela Mingarelli, Sai Sakktee Krisna, Dakota Rogers, Dr. Marija Landekic, and really everyone on the 3rd floor Bellini for both giving me feedback and advice when I was stuck on experiments and for sharing pitchers of refreshments after a long day's work. It was a pleasure working alongside all of you.

Author contributions

Benoit Charbonneau helped carry out *in vivo* mouse infections and necropsies. He also assisted me in performing plaque assays as well as sample processing for RNA extraction. Dr Mitra Yousefi helped plan and do the mouse infections and necropsies and managed all aspects BSL3 related. Patricia Caroline D'Arcy did the mouse infections and necropsies with the help of Benoit Charbonneau, Dr. Mitra Yousefi, and myself. Dr. Bin Gu and Dr. Lauryl Nutter led the efforts to generate and validate the CD-1 human angiotensin converting enzyme 2 (*hACE2*) knock-in (KI) mouse model. Jesse Islam helped immensely in processing the raw RNA-seq data reads, guiding me through the genpipes rnaseq.py pipeline as well as setting up and troubleshooting the R analysis along with input from HanChen Wang, and Dr. Mathieu Mancini. Thank you all for helping me complete this project.

My own contributions include running all sample processing (e.g.: RNA extraction), plaque assays, genotyping mice, setting up animal experiments, quantitative polymerase chain reaction (qPCR), and all analysis and processing of RNA-seq data.

List of Abbreviations

ACE2, Ace2: angiotensin converting enzyme 2

AD: Alzheimer's disease

ANOVA: analysis of variance

APC: antigen presenting cell

B6: C57BL/6

BP: biological processes

BSL3: biosafety level 3

CCL: C-C chemokine ligand

CCNA2: cyclin A2

CCR: C-C chemokine receptor

CD: cluster of differentiation

cDNA: complementary DNA

CL3: containment level 3

CMC: carboxymethyl cellulose

COPII: coated protein complex II

CPM: counts per million

CSF1R: colony-stimulating factor-1 receptor

CXCL: CXC chemokine ligand

COVID-19: coronavirus disease 2019

DAVID: Database for Annotation, Visualization and Integrated Discovery

DEG: differentially expressed genes

DMA: HLA-DM protein α

DMEM: (Gibco's) Dulbecco's Modified Eagle Medium

DMV: double membrane vesicles

DNA: deoxyribonucleic acid

dpi: days post-infection

DPP9: dipeptidyl peptidase 9

dsRNA: double-stranded RNA

ER: endoplasmic reticulum

FBS: fetal bovine serum

FC: fold-change

FDR: false discovery rate

Fig.: figure

GAPDH: glyceraldehyde-3-phosphate dehydrogenase

GO: gene ontology

GPCR: guanine nucleotide-binding protein-coupled receptor

GPVI: glycoprotein VI

GSEA: gene set enrichment analysis

GWAS: genome-wide association studies

hACE2: human ACE2

HCoV: human coronaviruses

HLA: human leukocyte antigen

IFIT: interferon induced proteins with tetratricopeptide repeats

IFN: interferon

IFNAR: interferon alpha and beta receptor subunit

IFNG, IFN-γ, Ifng: interferon gamma

IKBK: inhibitor of nuclear factor kappa B

IN: intranasally

Inf.: infected

IRF: interferon regulatory factor

ISG: interferon stimulated gene

ISGF: ISG factor

ISRE: interferon-sensitive response element

JAK: Janus kinase

hACE2: human angiotensin converting enzyme 2

K18: epithelial cell ytokeratin-18

KI: knock-in

KO: knock-out

LCK: lymphocyte-specific protein tyrosine kinase

LRR: leucine rich repeat

MAIT: mucosal-associated invariant T

MAPK: mitogen-activated protein kinase

MAVS: mitochondrial antiviral signaling protein

MCM4: minichromosome maintenance complex component 4

MDA5: melanoma differentiation-associated protein 5

MERS-CoV: Middle Eastern respiratory syndrome-related coronavirus

MHC: major histocompatibility complex

MOI: multiplicity of infection

mRNA: messenger RNA

MYD88: myeloid differentiation primary response 88

NCAM1: neural cell adhesion molecule 1

NES: normalized enrichment score

NF-κB: nuclear factor kappa B

NHP: non-human primates

NK: natural killer

NKT: natural killer T

NLRP3: NOD-, LRR- and pyrin domain-containing protein 3

NOD: nucleotide-binding and oligomerization domain

Non-inf.: non-infected

Nsp: non-structural proteins

NTPase: nucleoside-triphosphatase

OAS: 2'-5'-oligoadenylate synthetase

ORC: origin recognition complex

ORF: open reading frame

PAMP: pathogen-associated molecular pattern

PaO2/FiO2: ratio of arterial partial pressure of oxygen to fraction of inspired oxygen

PASC: post-acute sequelae of COVID-19

PBMC: peripheral blood mononuclear cell

PBS: phosphate buffer saline

PCR: polymerase chain reaction

PFU: plaque forming units

PKR: protein kinase R

PRIM1: DNA primase subunit 1

PRR : pathogen recognition receptor

PSMA4: proteasome 20S subunit alpha 4

PSMD10: 26S proteasome non-ATPase regulatory subunit 10

PTPN: protein tyrosine phosphatase non-receptor type

qPCR: quantitative polymerase chain reaction

RBD: receptor binding domain

RdRp: RNA-dependent RNA polymerase

RIG-I: retinoic acid-inducible gene I

RIN: RNA integrity number

RIP: receptor-interacting protein

ROUT: robust regression and outlier removal

RNA: ribonucleic acid

RNA-seq: RNA sequencing

rRNA: ribosomal RNA

RTC: replication-transcription complex

S: spike

SARS-CoV: severe acute respiratory syndrome coronavirus

SARS-CoV-2: severe acute respiratory syndrome coronavirus 2

scRNA-seq: single cell RNA sequencing

SIRP: signal regulatory protein

SNP: single nucleotide polymorphism

SOCS: suppressor of cytokine signalling

SpO2: oxygen saturation levels on room air at sea level

ssRNA: single-stranded RNA

STAR: spliced transcripts alignment to a reference

STAT: signal transducer and activator of transcription

TANK: TRAF family member-associated NF-κB activator

TBK1: TANK binding kinase 1

TCP: The Center for Phenogenomics

TCR: T cell receptor

Teff: effector T cell

Tg: transgenic

TICAM: TIR domain-containing adaptor molecule

TIR: toll-interleukin receptor

TLR: toll-like receptor

TMPRSS2: transmembrane serine protease 2

TNF: tumor necrosis factor

TRAF: tumor necrosis factor receptor–associated factor

TRAV1-2: T cell receptor (TCR) alpha variable 1-2

TRIF: TIR-domain-containing adapter-inducing interferon-β

TRIM: tripartite motif protein

TWAS: transcriptome-wide association studies

TYK: Tyrosine kinase

UNC93B1: uncoordinated 93 homolog B1

USP: universal stress protein

VoC: variant of concern

WHO: world health organization

WT: wild-type

ZAP: zinc-finger antiviral protein

ZBP1: Z-DNA-binding protein 1

List of Figures and Tables

Chapter I: Introduction and Literature Review

Biological/clinical context

Coronavirus disease 2019 (COVID-19) in humans is caused by infection with severe acute respiratory syndrome coronavirus 2 (SARS-CoV-2) virus. During the acute phase of COVID-19, humans have demonstrated a range of disease severity from asymptomatic, mild, moderate, severe, and critical, as well as variability in organ systems infected (Sarkesh et al., 2020). While the medical and scientific community has reasonably focused their attention on the severe and critical forms of COVID-19, mechanistic and medical knowledge is lacking in the milder disease severities.

The aforementioned is an alarming notion as the majority of infected individuals have asymptomatic or mild disease severities (Ma et al., 2021) that still holds the promise of serious risks to infected hosts. Immunological changes in decidual T cells and macrophages have been observed at the maternal-fetal interface in asymptomatic at delivery or mild disease severity during pregnancy relative to healthy pregnant women from which pregnancy complications may arise in infected women due to the resulting impairment of pathogen clearance, wound healing, and initiation of labor (Sureshchandra et al., 2022). Furthermore, debilitating and life-changing post-acute sequelae of COVID-19 (PASC) have been observed in patients with asymptomatic and mild disease severities in anywhere from 10% to 60% of observed individuals (Deer et al., 2021; Malkova et al., 2021; van Kessel et al., 2022). Finally, individuals with asymptomatic disease can be strong drivers of transmission and propagate SARS-CoV-2 in the population, presenting as a serious concern for designing effective public health strategies (Bai et al., 2020; Huff & Singh, 2020).

A lot can be learnt from transcriptomic, metabolomic, genomic, proteomic, and epidemiologic studies of infected humans or tissues and samples isolated therein for *in vitro* studies; however, *in vivo* mechanistic studies, an important next step in testing theoretical frameworks following observational or *in vitro* human studies, require carefully controlled experiments that are difficult to ethically carry out *in vivo* in humans. To help fill this gap in knowledge, animal models are required. Animal models are indispensable because they model *in vivo* hierarchies from the various cell types to tissues to organs to physiological systems.

Mouse models are a popular choice for numerous reasons: (1) many physiological systems behave similarly to the human analogs including the immune system; (2) there are numerous reagents and protocols available to generate transgenic mice, conduct *in vivo* infections, and perform transcriptomic and proteomic assessments; (3) many research facilities are already equipped to house mice and have established ethical guidelines and protocols for carrying out relevant research. Different mouse models can be used to study different clinical manifestations and immunological responses to SARS-CoV-2, hopefully mirroring what happens in different disease severities in humans.

Objective

Herein, we describe a novel CD-1 *hACE2* KI model and compare it to a described severe disease model to SARS-CoV-2 infection, the C57BL/6 (B6) epithelial cell cytokeratin-18 (K18)-*hACE2* transgenic (Tg) model.

Hypothesis

We hypothesized that the CD-1 *hACE2* KI model epitomizes a physiological mouse *ACE2* expression pattern that would have a milder disease severity relative to the B6 K18-*hACE2* Tg model.

Aims and Methodology

First, the differences in disease presentations between the two models were determined. Next, the early immune responses in the two models and how they differed between different disease severity outcomes was determined.

To accomplish the aims listed above, the following methodology was followed: (1) monitored disease phenotypes and established differences in clinical and sub-clinical phenotypes outcomes (body weight, clinical score, clinical biochemistry in plasma); (2) examined levels of virus load using viral qPCR and plaque assay from lungs; (3) studied global lung transcriptomic profiles at an early time-point (2 days post-infection (dpi)) and used pathway analysis to identify differentially expressed pathways and leading-edge analysis to predict molecular drivers of disease as well as examine similarities between infection models; (4) examined influence of viral load with host response by correlation analysis.

Comprehensive review of the relevant literature

On the road of a pandemic. In December 2019, cases of pneumonia of unknown etiology were reported in the Hubei province (Wang et al., 2020). Later, airway epithelial cells from infected patients were used to isolate a novel coronavirus, now termed SARS-CoV-2 (Wang et al., 2020). By March 11, 2020, the respiratory virus had spread to 114 countries, reporting 118,000 cases and 4,291 deaths and the World Health Organization (WHO) declared a pandemic (World Health Organization, 2020).

Since then, the world has had its hands full with the virus: there were tens of trillions of dollars of economic loss due to preventive health measures, premature deaths, and medical costs (Cutler & Summers, 2020); highly effective vaccines (e.g.: messenger (mRNA)-based vaccine Spikevax® or mRNA-1273 demonstrated an initial efficacy of 94.1% in preventing severe disease (Baden et al., 2021)) and therapies (e.g.: antiviral Paxlovid has 89% lower death or hospital admission for participants starting treatment within three days of COVID-19 symptom onset relative to the placebo group (Mahase, 2021)) were developed in a remarkably short time; variants of concern (VoCs) emerged that have increased immune evading properties as observed with the Omicron variant (B.1.1.529) having increased neutralization by serum and monoclonal antibodies against the spike protein (McCallum et al., 2022; Planas et al., 2021; Zhang et al., 2022). Such a remarkable scourge to the world deserves a closer look.

The genetic and molecular wirings of SARS-CoV-2. SARS-CoV-2 shares an almost 79% nucleotide similarity to severe acute respiratory coronavirus (SARS-CoV) (Lu et al., 2020). It belongs to the *Betacoronavirus* genus and *Sarbecovirus* subgenus, to which

SARS-CoV also belongs (Abdelrahman et al., 2020). All previous human coronaviruses including endemic human coronaviruses (HCoVs) (e.g.: HCoV-OC43, HCoV-NL63, HCoV-229E, and HCoV-HKU1) (Corman et al., 2018), SARS-CoV, and Middle East respiratory syndrome-related coronavirus (MERS-CoV) have zoonotic origins (Holmes et al., 2021). Based on the current data, SARS-CoV-2 also appears to have a zoonotic origin; several bat viruses (RmYN02, RpYN06, and PrC31) have strong nucleotide similarity to the open reading frame (ORF) 1ab (ORF1ab) of SARS-CoV-2 (Li et al., 2021; Lytras et al., 2022; H. Zhou et al., 2021); in addition, that many initial confirmed cases cluster around the Huanan live animal markets (Chen et al., 2020) combined with the emergence of two early phylogenetic lineages (A and B) (Rambaut et al., 2020) hints towards multiple spill-over-events (Holmes et al., 2021).

Molecularly, SARS-CoV-2 is a positive sense RNA virus with a genome of around 29.9 kb (Brant et al., 2021). The genome is organized into various open reading frames (ORFs): ORF1a and 1ab encodes for non-structural proteins (nsp) nsp1 to nsp16 which includes the RNA-dependent RNA polymerase (RdRp); ORF2 to 10 encodes for structural proteins including the surface glycoprotein spike (S), membrane integral envelope protein, membrane glycoprotein, and genome organizing and RNA stabilizing nucleocapsid protein as well as accessory proteins (Brant et al., 2021).

S is crucial for viral cell entry; each subunit of this homotrimer is composed of an S1 and S2 subunit (Jackson et al., 2022). S1 contains the receptor binding domain (RBD) that is crucial for binding the cognate host receptor ACE2 and initial attachment (Jackson et al., 2022). Afterwards, two cleavages are necessary for membrane fusion (Jackson et al., 2022; Örd et al., 2020). First, the S1-S2 furin site must be cleaved by furin or host

transmembrane serine protease 2 (TMPRSS2). The first cleavage allows access to the S2' site for cleavage by surface TMPRSS2 or endosomal cathepsins (e.g.: cathepsin L), to release the fusion machinery within the S2 subunit, allowing membrane fusion (Jackson et al., 2022; Örd et al., 2020).

Following cell entry, host ribosome translates the ORF1a and ORF1ab reading frames into polyprotein pp1a and pp1ab (Yan et al., 2022). Proteolytic cleavage by viral encoded proteases frees up all 16 non-structural proteins Nsp1 to Nsp16. The RdRp or Nsp12 along with nsp7, nsp8, nsp9, and 2 molecules of nsp13 (helicase and nucleoside-triphosphatase (NTPase)) combine to form the replication-transcription complex (RTC) at double membrane vesicles (DMV) at the surface of endoplasmic reticulum (ER) wherein viral replication occurs (Malone et al., 2022; Wolff et al., 2020; Yan et al., 2022). Notably, SARS-COV-2's nsp14 or exonuclease protein allows for proofreading activity, greatly reducing the error rate during replication (Tahir, 2021). Genomic replication occurs through the production of negative-sense intermediates (Malone et al., 2022; Yan et al., 2022). Furthermore, the translation of structural and accessory viral proteins (ORF2 to 10), many of which are required for proper virion assembly, requires the production of subgenomic intermediates that contain a common leader sequence important for protection against cleavage by nsp1, a host translation inhibition factor (Schubert et al., 2020), and for priming subgenomic viral mRNAs (Finkel et al., 2021; Hartenian et al., 2020). Having described potential origins, genome structure, and virus entry and replication, how does this virus affect humans?

How bad do you have it: very sick, sick, or not sick at all. In humans, SARS-CoV-2 causes coronavirus disease 2019 (COVID-19). Disease severity can manifest as critical if there is “respiratory failure, septic shock, and/or multiple organ dysfunction” ("Coronavirus Disease 2019 (COVID-19) Treatment Guidelines," 2021); severe forms require hospitalization and mechanical air ventilation in individuals with oxygen saturation levels on room air at sea level (SpO_2) < 94%, ratio of arterial partial pressure of oxygen to fraction of inspired oxygen (PaO_2/FiO_2) < 300 mm Hg, > 30 breaths/minute, or > 50% lung infiltrates ("Coronavirus Disease 2019 (COVID-19) Treatment Guidelines," 2021); individuals might have moderate disease severity where there is evidence of lower respiratory disease; mild disease severity occurs when any number of symptoms (e.g.: fever, cough, sore throat, headache, muscle pain, nausea, vomiting, diarrhea, and loss of taste and smell) are present but without lower respiratory disease ("Coronavirus Disease 2019 (COVID-19) Treatment Guidelines," 2021; Sarkesh et al., 2020).

There is a fifth category of disease severity, the asymptomatic type, where individuals test positive for SARS-CoV-2 infection by antigen or nucleic acid presence but without any of the symptoms described above ("Coronavirus Disease 2019 (COVID-19) Treatment Guidelines," 2021). Asymptomatic and mild disease severity might represent altogether as much as 90% of total infectious cases (Alene et al., 2021; Auwaerter, 2022; Ma et al., 2021). Because asymptomatic individuals can still present risks during pregnancy (Sureshchandra et al., 2022), or present with PASC (Deer et al., 2021; Malkova et al., 2021; van Kessel et al., 2022), and contribute heavily in human-to-human transmission (Bai et al., 2020; Huff & Singh, 2020), a closer examination and study is warranted.

Underneath the nothingness. While all ages are susceptible to asymptomatic COVID-19, elderly people (over 65 years of age) are more likely to present with symptoms later on during the course of infection compared to younger (e.g.: children under 18 years of age) individuals (You et al., 2021). Concerning the ancestral Wuhan strain (February 2020) of the virus, it has a similar level of peak viral load early during infection in both symptomatic and asymptomatic individuals (Zou et al., 2020); asymptomatic individuals also had a longer duration of viral shedding (median 19 days, as determined by nucleic acid detection) relative to symptomatic individuals (Long et al., 2020), altogether supporting the theory of high potential spread from asymptomatic individuals (Bai et al., 2020; Huff & Singh, 2020).

Immunologically, there are conflicting data in the literature. One study noted that there was no significant difference in blood protein markers, cell immune profiles, or peripheral blood mononuclear cells' (PBMCs) transcriptomics between asymptomatic seropositive individuals compared to seronegative individuals while mild symptomatic individuals had evidence of a proinflammatory immune signature in an Austrian community (Lee et al., 2020).

On the other hand, two single-cell RNA-seq (scRNA-seq) study on PBMC samples from a variety of disease severity individuals noted several immunological changes in asymptomatic relative to symptomatic, moderate, and severe disease severity individuals and yet different compared to healthy uninfected individuals, making the case of a unique immunological signature in asymptomatic COVID-19 infected people. Asymptomatic individuals had (1) increased cluster of differentiation (CD) 56 $(CD56)^{bri}$ $CD16^{-}$ natural killer (NK) cells, T cell receptor (TCR) alpha variable 1-2 $(TRAV1\text{-}2)^{+}CD8^{+}$ mucosal-

associated invariant T (MAIT) cells, $CD4^{lo}$ colony-stimulating factor-1 receptor $(CSF1R)^{-}$ $CD33^{-}CD14^{+}$ & $CD33^{-}$ human leukocyte antigen $(HLA)^{-}$ HLA-DM protein α $(DMA)^{-}CD14^{+}$ classical monocytes, and neural cell adhesion molecule 1 $(NCAM1)^{hi}CD160^{+}$ natural killer T (NKT) cells, (2) increased interferon (IFN) gamma (IFNG) in effector T (T_{eff}) $CD4^{+}$ and $CD8^{+}$ cells and NK cells, (3) strong $CD4^{+}$ T cell clonal expansion, (4) weak B cell clonal expansion, and (5) lower interferon stimulate genes (ISGs) expression overall with higher interindividual variability (Wang et al., 2022; Zhao et al., 2021).

Supporting evidence from a PBMC RNA-seq study identified lower IFN response and complement activation from gene set enrichment analysis (GSEA) in asymptomatic relative to symptomatic individuals (Zhang et al., 2021). Two studies demonstrated lower antibody titers or an absence of seroconversion as well as a lower magnitude of cell-mediated (i.e.: virus reactive T cells) in asymptomatic compared to symptomatic individuals (Long et al., 2020; Mazzoni et al., 2020; Shirin et al., 2020). A larger proportion of asymptomatic individuals became seronegative or decreased in neutralization titers compared to a symptomatic cohort in the early convalescent phase (Long et al., 2020). Asymptomatic individuals also had lower levels of several pro- and anti-inflammatory blood cytokines (Long et al., 2020).

Altogether, the evidence seems to point towards a unique yet present immune response that is weaker in magnitude in asymptomatic compared to symptomatic individuals. However, most data reported in humans comes from either blood cytokines or *ex vivo* PBMC assays and analysis as other tissue's samples are difficult to obtain. Mechanistic understanding of asymptomatic disease and pathogenesis, especially at a

multi-organ level is difficult to gain from such samples; for such knowledge, models and especially animal models are required.

Not the real thing-so why bother? The use of animal model in medical and scientific research is a controversial subject. While there are many similarities in physiological systems between humans and other mammals, many findings from animal studies modeling stroke and cancer do not translate to successful treatments in humans, perhaps owing to failures in recapitulating human disease progression and complexity (Akhtar, 2015; Frangogiannis, 2022; Mak et al., 2014; Wendler & Wehling, 2010). Perhaps most famous is the inability to reproduce the results of top drug candidates and strategies validated in animal models of Alzheimer's disease (AD) in humans, although this may also be due to incorrect or insufficient underlying pathophysiological mechanisms of AD modeled in these animal models (Van Dam & De Deyn, 2011).

Nevertheless, many successes have also resulted from the use of animal models. Surgical knowledge including the development of tracheostomy (Haddad, 2004; Litynski, 1997) and surgery for treating tetralogy of Fallot (Timmermans, 2003) were developed with the help of animal models (Robinson et al., 2019). Vaccine development is another area where animal models shine; monkeys were used to develop the polio vaccine (Sabin, 1965) and animal models from mice to non-human primates (NHPs) were used to develop vaccines for COVID-19 (Muñoz-Fontela et al., 2020; Robinson et al., 2019).

As others have discussed (Akhtar, 2015; Frangogiannis, 2022; Mak et al., 2014; Wendler & Wehling, 2010), the intentions and limitations of animal models must always be considered and when used appropriately, a lot can be learnt. The use of both inbred

and outbred strains allows for the minimization of genetic variability; to add, the careful use of appropriate control groups and/or Tg knock-out or gain-of function constructs can allow for deep mechanistic understanding. Knowing this, what animal models are currently available to study COVID-19?

Making animals sick. Numerous animal models for COVID-19 have been developed. Syrian golden hamsters present with age-associated disease severity and virus dose-dependent disease severity (Imai et al., 2020). Ferrets are often used in transmission studies, displaying mild infection, and having viral RNA at higher levels in upper respiratory tract compared to lower respiratory tract (Richard et al., 2020). NHPs (e.g.: rhesus macaques, African green monkeys, and baboons) have also been studied; they present with heterogenous responses ranging from mild to moderate lung pathology (inflammation and immune cell infiltration) (Singh et al., 2021; Woolsey et al., 2021). Most NHPs recover from the disease, and they are often used for testing therapeutics and vaccines (Singh et al., 2021; Woolsey et al., 2021). All the abovementioned animal models have advantages and uses as COVID-19 models; however, murine models have the advantage of numerous reagents and protocols being available (especially the generation of genetically modified animals) and most animal facilities are already equipped to handle mice.

Most mouse models for SARS-CoV-2 infection seek to introduce *hACE2* as the original Wuhan isolate of SARS-CoV-2 virus cannot infect mouse *ACE2*. One versatile approach is using viral vectors (adenovirus type-5 and adeno-associated virus) to introduce *hACE2* that has been used on backgrounds of B6 and BALB/c as well as

various knock-out (KO) strains; this model presents with mild disease at high inoculum doses (e.g.: up to $1x10^7$ plaque forming units (PFU) per mouse) and allows researchers to gain insight on immune cell numbers and transcriptomics (Israelow et al., 2020; J. Sun et al., 2020). KI *hACE2* models in B6 have been developed that have the advantage of using the endogenous mouse promoter and present with mild disease (S. H. Sun et al., 2020). Certain groups have also used mouse adapted virus with engineered amino acid residues that was passaged several times in BALB/c mice (by infecting mice, isolating viral homogenates, and infecting more mice) (Leist et al., 2020); this adapted virus was capable of infecting BALB/c mice that later presented with age-associated disease severity (Leist et al., 2020). Finally, the B6 K18-*hACE2* transgenic mice (hereafter referred to as B6 Tg) mice are emerging as the standard severe disease model. These mice have shown around 40% encephalitis that is not associated with the near 100% mortality rate in most studies with doses greater than 10,000 PFU (Winkler et al., 2020; Yinda et al., 2021). As mentioned previously, what's remarkable is that disease variability is observed in both humans and mouse models so it's worth considering what are the molecular pathways that are suspected or known to be involved in SARS-CoV-2 host defense.

Many pathways for different severities. The interpersonal variability in disease severity is in part due to the genetics and early host response of infected individuals. In support of this idea, several genome-wide association studies (GWAS) and transcriptome-wide association studies (TWAS) have identified genes that, when deficient or have defective products, are associated with increased risk of severe disease. Candidate genes include

interferon alpha and beta receptor subunit 2 (*IFNAR2*), tyrosine kinase 2 (*TYK2*), 2'-5'-oligoadenylate synthetase 1 (*OAS1*), *OAS2*, *OAS3*, dipeptidyl peptidase 9 (*DPP9*), and C-C chemokine receptor type 2 (*CCR2*) (Pairo-Castineira et al., 2021). A large collaborative effort also found autosomal recessive genetic defects (interferon regulatory factor 7 (*IRF7*) & *IFNAR1*) or autosomal dominant genetic defects (toll-like receptor 3 (*TLR3*), toll-interleukin receptor (TIR) domain-containing adaptor molecule 1 (*TICAM1*), tumor necrosis factor receptor–associated factor (TRAF) family member-associated nuclear factor kappa B (NF-κB) activator (TANK) binding kinase 1 (*TBK1*), *IRF3*, uncoordinated 93 homolog B1 (*UNC93B1*), *IRF7*, *IFNAR1*, and *IFNAR2*) in critical COVID-19 patients that represented 3.5% of their cohort (Zhang et al., 2020). Furthermore, Mendelian randomization studies have found loci that associate with changes in the expression of certain gene products and that these changes associate with disease severity differences (Evans & Davey Smith, 2015). For example, a Neanderthal *OAS1* isoform found in ethnic European ancestry was associated with increased OAS1 levels and associated with reduced COVID-19 death, hospitalization, and susceptibility (S. Zhou et al., 2021). In addition, Bastard et al. observed autoantibodies against type 1 interferon in approximately 10% of a severe COVID-19 cohort, most of whom are men (Bastard et al., 2020). Many of the identified genes and loci are involved in the early innate immune response, including interferon production, interferon signaling, and pathogen recognition pathways.

Sensing pathogens-and what's next? Various type of pathogen recognition receptors (PRRs) recognize different pathogen-associated molecular patterns (PAMPs) (e.g.:

nucleic acids, adenosine triphosphate, and lipopolysaccharide) that may be present both on cellular membranes (at the plasma membrane or within endosomal compartments) or in the cytoplasm (Tang et al., 2012). Concerning RNA viruses, endosomal receptors include TLR3 (double-stranded (dsRNA) sensor), TLR8 (single-stranded (ssRNA) sensor), and TLR7 (ssRNA and dsRNA sensor) are available, signaling with downstream TIR-domain-containing adapter-inducing interferon-β (TRIF), myeloid differentiation primary response 88 (MYD88), and MYD88 adaptors, respectively (Schlee & Hartmann, 2016). These signal through IRF3/7 and NF-κB to either transcriptionally produce type 1 interferons (*IFNα* and *IFNβ*), pro-inflammatory cytokines, and/or nucleotide-binding and oligomerization domain (NOD)-, leucine rich repeat (LRR)- and pyrin domain-containing protein 3 (*NLRP3*) and pro-interleukin (IL) 1β *(IL-1β*), unleashing interferon, pro-inflammatory, and/or pro-cell death pathways (Jensen & Thomsen, 2012; Schlee & Hartmann, 2016).

In terms of cytoplasmic RNA viruses, retinoic acid-inducible gene I (RIG-I), melanoma differentiation-associated protein 5 (MDA5), and OAS1 can recognize dsRNA (Schlee & Hartmann, 2016). OAS1 can degrade dsRNA through activation of RNAse L (Schlee & Hartmann, 2016). On the other hand, RIG-I and MDA5 signal through mitochondrial antiviral signaling protein (MAVS) to either activate the NLRP3 inflammasome, initiate an apoptosis program, and/or signal through IRF3/7 and NF-κB to produce transcripts for type 1 interferons, pro-inflammatory cytokines, and/or pro-apoptosis pathways' proteins (Jensen & Thomsen, 2012; Schlee & Hartmann, 2016).

While SARS-CoV-2 is a positive ssRNA virus, it undergoes a temporary dsRNA intermediate during replication that may be recognized by dsRNA sensors, although the

intermediate complex is purported to be shielded in the DMVs found in the ER (as of yet unconfirmed, however) (V'kovski et al., 2021; Wolff et al., 2020).

The interferon signaling pathway is online. Type I interferons encompass a large class of proteins including IFN-α, -β, -ε, -κ, and -ω (Platanias, 2005). They signal through IFNAR1 and IFNAR2 heterodimers that associate with TYK2 and Janus kinase 1 (JAK1) tyrosine kinases. These phosphorylate signal transducer and activator of transcription (STAT) proteins to form either STAT1 homodimers and/or STAT1/2 heterodimers. Activated STAT1/2 can form a complex with IRF9 to form interferon-stimulated gene factor 3 (ISGF3) to transcriptionally activate various interferon-sensitive response elements (ISREs) and transcribe various interferon-stimulated genes ISGs. In total, from microarray studies, humans express anywhere between 50-1000 ISGs per cell (200-500 typical) (Schoggins & Rice, 2011)! The protein expressed form of ISGs have a wide arrange of functions to combat viral infection, including: (i) enhanced sensitization to pathogen sensing, through increased expression of PRRs and IRFs; (ii) desensitization to IFN, through the production of suppressor of cytokine signalling (SOCS) proteins and universal stress protein (USP) 18 (USP18), for example, (iii) antiviral effectors, including inhibitors of viral entry such as interferon induced proteins with tetratricopeptide repeats (IFIT) proteins and Mx proteins; inhibitors of virus translation and replication, such as zinc-finger antiviral protein (ZAP), OAS, RNAse L, protein kinase R (PKR), and inhibitors of viral egress, including viperin and tetherin (Schneider et al., 2014). During infection, the vast array of ISGs come online depending on cell type, IFN dose, and timing (Schoggins & Rice, 2011).

Chapter 2: Materials and Methods

Viral stock production. A clinical viral isolate (isolated prior to November 2020) termed SARS-CoV-2 CP13.32 P4 passage 2 (Genbank accession no. 599736; lineage B1.1.147) stock was kindly obtained from the McGill University Health Center (with special thanks to Mitra Yousefi and the McGill containment level 3 (CL3) facility) from which the CP13.32 P4 passage 3 to passage 4 stocks were made for mouse infections. The clinical isolate bears strong similarity to the Wuhan-Hu-1 sequence NC_045512, contains the widespread (by end of March 2020) D614G amino acid change (Korber et al., 2020), and was obtained prior to the emergence of the various VoCs. A list of amino acid changes and mutations in passages 4 and 2 relative to the NC_045512 sequence is presented in **Supplementary Table 2**.

Briefly, on day 0, T175 flasks with VeroE6 cells were grown to between $1.2x10^7$ to $1.4x10^7$ cells/flask in 10% fetal bovine serum (FBS) and 1% penicillin/streptomycin Dulbecco's Modified Eagle Medium (DMEM) media (seeded at $3.5x10^6$ cells/flask 48 hours prior). Media was changed to 10 mL of phosphate buffer saline (PBS) during transport to BSL3 facility (under 1 hour). PBS was removed and 5 mL of original viral stock inoculum was seeded at a multiplicity of infection (MOI) of 0.03 for passaged viral stock or plain DMEM for mock viral inoculums. Flasks were incubated at 37 °C for 1 hour and shaken crosswise every 15 minutes after which inoculum was removed and 25 mL of 2% FBS DMEM media added.

At 2 dpi, infected media was collected and spun through pre-wet (with plain DMEM) 100 kDA Amicon filters at 1699 g for 5 minutes at 4 °C (twice, 12.5 mL at a time per flask) and flow-through was discarded. Volume in the insert of the filter was resuspended to 1 mL

per tube for a 25-fold concentration factor. The concentrated virus was later titrated and used for mouse infections.

Mouse infections. Mice used for SARS-CoV-2 infections included C57BL/6 wild-type (WT) and C57BL/6 K18-*hACE2* hemizygous transgenic mice purchased from Jackson Laboratories (Bar Harbor, ME, USA) and bred in-house with guidance from McGill University's animal facility institution approval. CD-1 WT and CD-1 *hACE2* KI hemizygous mice were kindly given for this study by TCP.

Briefly, infections were carried out in the BSL3 laboratory located at McGill University. Mice were transported to the BSL3 facility the night before the experiment to reduce animal stress. Mice were first anesthetized via intraperitoneal administration of ketamine and xylazine and either 250,000 PFU for CD-1 WT and CD-1 *hACE2* KI or 50,000 PFU for C57BL/6 WT and C57BL/6 K18-*hACE2* hemizygous was administered intranasally (IN) in a 20 µL inoculum. Mice were monitored until recovery from infection and anesthesia (around 2 hours) and afterwards monitored twice daily starting from 3 days post-infection.

A first 14-day survival cohort consisted of 5 WT and 5 Tg or KI mice for both B6 and CD-1, respectively. A second day 2 post-infection cohort consisted of 5 WT and 5 Tg or KI mice for both B6 and CD-1, respectively. The 2 day-post infection cohort underwent necropsy to recover lungs for plaque assay (right lung) and RNA assays (qPCR and RNA-seq for left lung) whereas plasma was obtained for cytokine protein level multiplex analysis.

Plaque assays. VeroE6 cells were grown in 12-well plates seeded at a density of $7.50x10^4$ cells/mL 72 hours before or $1.50x10^5$ cells/mL 48 hours before the day 0 infection. Cells were passed through a 40 µM filter and shaken thoroughly to prevent clotting or aggregation of the cells.

At day 0 (infection), frozen lungs -80 °C (taken on the day of necropsy) were homogenized and clarified twice (remove supernatant and spin at 12,000 g for 10 mins at 4 °C). Serial dilutions of 0.5-, 10^{-1}-, 10^{-2}-, 10^{-3}-, 10^{-4}-, and 10^{-5}-fold were made. To the VeroE6 cells, media was changed to 0.5 mL of 2% FBS DMEM media during transport to BSL3 facility (under 1 hour). Media was removed and 0.2 mL of each viral dilution was added per well, in duplicate. Cells were incubated at 37 °C for 1 hour and shaken crosswise every 15 minutes after which inoculum was removed and 0.5 mL of 6% carboxymethyl cellulose (CMC) and 2% FBS in DMEM was added.

At day 3 post inoculation, CMC was removed, and 3 mL of 4% formalin was added to each well. The formalin was left for 1 hour (to allow for both fixation and virus inactivation). Formalin was removed and 0.2% crystal violet in 70% ethanol was added for 10 minutes. Staining was removed and washed with distilled water. The plaques were visible the following day.

Plasma cytokine multiplex assay. Plasma was obtained by addition to ethylenediaminetetraacetic acid tubes and spun at 3000 g for 10 minutes at room temperature. Plasma was virus-inactivated by addition of 1% Triton X-100 in PBS 1:9 in plasma that was left for 1 hour at room temperature. Samples were shipped to Eve Technologies (Calgary, AB, CA) for the Mouse Cytokine 44-Plex Discovery Assay.

RNA extraction and clean-up. Lung samples were sectioned and added to RNAlater™ (Thermo Fisher Scientific) and kept on an ice block (at -20 °C) during necropsy, immediately being stored at -20 °C afterwards. Within 2-weeks, tissues were removed and added to 1 mL TRIZOL (Thermo Fisher Scientific). Following homogenization and 2 rounds of clarification, RNA was extracted using the classic TRIZOL method: addition of chloroform, extraction of aqueous phase, sequential addition and removal of isopropyl alcohol and alcohol, and finally pellet drying. Next, samples underwent DNase I (Sigma) treatment at a cycle of 37 °C for 15 minutes and 95 °C for 10 minutes. For RNA-seq clean-up only, RNA samples underwent purification step using the Quick-RNA™ MicroPrep kit (Zymogen) before proceeding to analysis and library preparation.

Quantitative polymerase chain reaction (qPCR). Isolated RNA underwent reverse transcription using the M-MLV reverse transcriptase kit (Invitrogen™). 4-fold diluted complementary deoxyribonucleic acid (DNA) (cDNA) underwent qPCR at a cycle 95 °C for 10 minutes followed by 40 cycles of 95 °C for 10 seconds, 60 °C for 20 seconds, and 70 °C for 15 seconds (read fluorescence here). Primer sequences are described below:

Isg15

F_Primer: AGAGCCTGCAGCAATGGC

R_Primer: TCGCTGCAGTTCTGTACCA

Usp18

F_Primer: CGTGCTTGAGAGGGTCATTT

R_Primer: GGTCGGGAGTCCACAACTTC

Cxcl10

F_Primer: ATCATCCCTGCGAGCCTATCCT

R_Primer: GACCTTTTTTGGCTAAACGCTTTC

Gapdh

F_Primer: TCCACCACCCTGTTGCTGTA;

R_Primer: TCCACCACCCTGTTGCTGTA)

SARS-CoV-2 nucleocapsid (N)

F_Primer: TAATACGACTCACTATAGGGAAATTTTGGGGACCAGGAAC

R_Primer: TGGCAGCTGTGTAGGTCAAC)

RNA-sequencing, data processing and differentially expressed gene (DEG) analysis. RNA samples were sent to Genome Quebec (Montreal, QC, CA) for RNA-seq. RNA samples were used if RNA integrity number (RIN) > 6.0 and n=5 passed for all groups except for n=4 for B6 WT non-infected (non-inf.), n=4 for CD-1 WT infected (inf.), and n=3 for CD-1 KI non-inf. due to inferior RNA quality. Following ribosomal RNA (rRNA) depletion, cDNA libraries were constructed by Genome Quebec as follows next. Briefly, total RNA was quantified using a NanoDrop Spectrophotometer ND-1000 (NanoDrop

Technologies, Inc.) and its integrity was assessed on a LabChip GXII instrument (PerkinElmer). rRNA was depleted from 125 ng of total RNA using QIAseq FastSelect (Human/Mouse/Rat 96 reactions). cDNA synthesis was achieved with the NEBNext RNA First Strand Synthesis and NEBNext Ultra Directional RNA Second Strand Synthesis Modules (New England BioLabs). The remaining steps of library preparation were done using and the NEBNext Ultra II DNA Library Prep Kit for Illumina (New England BioLabs). Adapters and polymerase chain reaction (PCR) primers were purchased from New England BioLabs. Libraries were quantified Kapa Illumina GA with Revised Primers-SYBR Fast Universal kit (Kapa Biosystems). Average size fragment was determined using a LabChip GXII instrument (PerkinElmer).

The libraries were normalized and pooled and then denatured in 0.05N NaOH and neutralized using HT1 buffer. The pool was loaded at 225 pM on an Illumina NovaSeq S4 lane using Xp protocol as per the manufacturer's recommendations. The run was performed for 2x100 cycles (paired-end mode). A phiX library was used as a control and mixed with libraries at 1% level. Base calling was performed with RTA v3.4.4 program bcl2fastq2 v2.20 was then used to demultiplex samples and generate fastq reads.

Processing was done on the rnaseq.py pipeline from genpipes (Mathieu Bourgey et al., 2019) using the base code with Trimmomatic (Bolger et al., 2014) arguments TRAILING: 30, MINLEN: 32, and HEADCROP: 10 followed by spliced transcripts alignment to a reference (STAR) alignment (Dobin et al., 2013) to the GRCm38 mouse genome, with stringtie (Pertea et al., 2015) count assembly and count determination with featureCounts (Liao et al., 2013). After filtering for a counts per million (CPM)> 5 in 5 samples to consider a gene as detected, differential gene expression was calculated

using DESeq2 (Love et al., 2014), using infection status (inf. vs. non-inf.), mouse strain (B6 or CD-1), and transgenic construct (KI, Tg, or WT) as covariates. Primary analysis comparisons consisted of comparing CD-1 KI inf. vs. non-inf. and B6 Tg inf. vs. non-inf. mice to control for strain-specific differences. Genes with an adjusted p-value cut-off of less than 0.05 were considered a DEG.

Gene ontology (GO) term analysis. For viral correlation GO term analysis, biological processes (BP) GO terms are displayed for the significantly correlated genes (p-value < 0.05) in the different categories. For host response GO term analysis, BP GO terms are displayed for significantly (adjusted p-value < 0.05) either unique up (fold-change (FC) > 0) or down (FC < 0), or concordant or discordant gene (up in one model, down in other) categories. GO terms for different gene sets were calculated using the Database for Annotation, Visualization and Integrated Discovery (DAVID) software (Huang da et al., 2009; Sherman et al., 2022). Only GO terms with at least one parent hierarchy tree of level 8 or greater were considered to filter for biologically specific GO terms and with and false discovery rate (FDR) value cut-off of less than 0.05.

Gene set enrichment analysis (GSEA) and leading edge gene analysis. Gene set enrichment analysis was done using GSEA_4.2.3 software from Broad Institute (Mootha et al., 2003; Subramanian, Tamayo, Mootha Vamsi, et al., 2005). Normalized CPM matrices were used with C2.CP.Reactome.v7.5.1 gene sets. Settings were 1000 permutations, using weighted enrichment statistic and Signal2Noise metric for ranking

genes. Gene list was sorted with “real” setting and in descending order. Minimum and maximum size of sets were 15 and 500, respectively.

Leading edge gene analysis was done on the same software to find genes which contributed the most to the enrichment signal as done previously (Fleming & Miller, 2016) of selected gene sets (either common gene sets for **Fig. 4** and uniquely significant or discordant (e.g.: opposite sign of NES scores in one model compared to another) gene sets for **Fig. 6**) in both B6 Tg inf. vs. non-inf. and CD-1 KI inf. vs. non-inf. comparison cases. Genes were classified based on the number of gene sets for which they contributed to the enrichment. As numerous genes contribute to the enrichment signal in all gene sets considered, thresholds were set to reduce the number of candidate leading edge genes. Considering leading edge genes in common gene sets in **Fig. 3**, either of (i) 4 gene sets in either infection model or (ii) difference of 3 gene sets counts between models (e.g.: 3 gene sets in the B6 infection model and 0 gene sets in the CD-1 infection model). Considering leading edge genes in unique or discordant gene sets in **Fig. 6**, thresholds for consideration as a leading edge gene was contribution to enrichment in 4 gene sets or more in either infection model.

Statistical methods. All statistics were calculated with GraphPad Prism. Presence of outliers was verified with robust regression and outlier removal (ROUT) Q=1%. Normality assumptions were tested using both Shapiro-Wilk’s test for normality and graphically with Q-Q plots for CD-1 and B6 mouse strain comparisons separately. For comparisons where number of mice (n) per group are equal, if passed gaussian distribution, one-way analysis of variance (ANOVA) test with Tukey’s multiple comparison

test was used. For comparisons where number of mice (n) per group are not equal, if passed gaussian distribution, Brown-Forsythe's one-way ANOVA test with Dunnett's T3 multiple comparison test was used, otherwise Kruskal-Wallis with Dunn's multiple comparison test was used for normality failed mouse groups. For plasma cytokines and plaque assay statistical tests, WT inf. and Tg or KI inf. (for B6 and CD-1, respectively) groups are compared directly with unpaired t test when number of mice (n) per group are equal and normality condition has passed or Welch's t test when number of mice per group are unequal and normality condition has passed.

Chapter 3: Results

The CD-1 KI mouse model presents as a mild disease severity model relative to the B6 Tg model of severe COVID-19. The 14-day survival experiment showed that all the B6 Tg mice (50,000 PFU given IN) progressively lost weight and displayed clinical manifestations (ruffled fur, inactivity, and hunched posture), reaching clinical endpoint by day 6 (**Fig. 1a-b**) while all the CD-1 KI mice (250,000 PFU given IN) did not lose weight or show clinical manifestations up to 14 dpi (**Fig. 1a-b**). These results suggested that the CD-1 KI has a milder disease severity relative to the B6 Tg severe disease model.

Concerning viral load, at 2 dpi in the lungs, there was $2.06 \pm 1.22 \times 10^7$ PFU/g of lung in the B6 Tg mice compared to $3.45 \pm 1.01 \times 10^4$ PFU/g of lung in the CD-1 KI mice (**Fig. 1c**). Assessed by qPCR, at 2 dpi in the lungs, there was $2.86 \pm 1.17 \times 10^4$ and $5.87 \pm 3.57 \times 10^2$ SARS-CoV-2 nucleocapsid gene relative expression to glyceraldehyde-3-phosphate dehydrogenase (*Gapdh*) in B6 Tg mice and CD-1 KI, respectively (**Fig. 1d**). The high viral load in the B6 Tg mice fits with the observed severe disease and lethality. Surprisingly, the CD-1 KI mice have infectious viral particles at 2 dpi (albeit a much lower amount than the B6 Tg) despite no observed symptoms, weight loss, or lethality in the survival cohort, giving the indication that the CD-1 KI model might indeed be asymptomatic rather than non-susceptible to viral infection and proliferation. This may at least in part be due to the nearly 20-fold lower *hACE2* CPM (**Fig. 1e**) expression in the lungs of CD-1 KI mice relative to B6 Tg mice as well as other tissues potentially (including upper airway and brain) (Shuai et al., 2021). Despite these considerations, after this preliminary assessment of disease presentations, the early immune response was

interrogated to look for genes or molecular pathways that might explain disease severity differences between the two models.

Similarities in pathogen recognition and interferon pathways during CD-1 KI and B6 Tg infection. When looking at the plasma cytokines, only CXC chemokine ligand (CXCL) 10 (CXCL10 or IP-10) and IL-6 are significantly increased at the protein level at 2 dpi in B6 Tg inf. vs. B6 WT inf. (**Supplementary Fig. 2g**), likely because it is too early in the course of infection to encounter plasma protein-level changes. Interestingly, IL-10 is down in CD-1 KI inf. vs. CD-1 WT inf. We thought the transcription changes at the lungs might be more indicative of the host response.

In both CD-1 KI and B6 Tg, there is significant upregulation of *Cxcl10* (**Fig. 2a**) and ISGs *Isg15* and *Usp18* (**Fig. 2a**) in the lungs at 2 dpi relative to non-inf. and WT groups. These results gave indication that by day 2, there was an immune response at least partially similar in nature elicited in both the B6 Tg and CD-1 KI models, however the depth and breadth of information regarding genes and molecular pathways driving disease differences was lacking using qPCR.

RNA-seq was performed to address these shortcomings and to answer two central questions: whether the (1) nature and/or (2) magnitude of host responses differed between the two models. To account for strain-specific differences, the main methodology involved comparing (1) inf. to non-inf. CD-1 KI mice, and (2) inf. to non-inf. B6 Tg mice. After doing various RNA-seq quality control (see **Supplementary Fig. 3a-b**) and filtering at a gene detection threshold of CPM > 5 for 5 samples, 14334 genes are detected. DEGs were then defined with DESeq2 (Love et al., 2014) as having an adjusted p-value < 0.05,

obtaining 1096 and 4086 DEGs for the CD-1 and B6 Tg infections, respectively. Mapping all genes and DEGs (**Fig. 2b-c**) showed that many top hit DEGs include ISGs such as *Mx1*, *Isg15*, *Oas1a*, and *Usp18* that were found significantly upregulated during both CD-1 KI and B6 Tg infection. However, there is lower significance, fold-change, and total number of DEGs in the CD-1 KI inf. vs. non-inf. compared to B6 Tg inf. vs. non-inf. comparison cases, providing a first hint that both the nature and magnitude of the host response might differ between the infections.

Next, lists of DEGs were compared between both CD-1 KI inf. and B6 Tg inf. case comparisons, revealing 715 shared DEGs (**Fig. 3a**). DEGs are considered unique if they are present (passed significance threshold) in the list of one comparison case and absent (did not pass significance threshold) in the second comparison case. Plotting these common DEGs by fold-change (**Fig. 3b**) revealed concordant and discordant gene expression patterns in both infection cases, with most genes having concordant up (FC > 0, 215 DEGs) or down (FC < 0, 466 DEGs) expression (**Fig. 3c**). BP GO term analysis was conducted on concordant up DEGs using DAVID (Huang da et al., 2009; Sherman et al., 2022) with an FDR < 0.05 and at least one parent hierarchy level greater than 8 criteria (to obtain biologically specific GO terms). Looking at selected terms revealed that many significant concordant upregulated pathways involved interferon signaling (i.e.: positive regulation of IFN-β production, negative regulation of viral entry into host cell, positive regulation of IFN-α production, and regulation of inhibitor of nuclear factor kappa B kinase (IκBK)/NF-κB signaling), early pathogen recognition (i.e.: cellular response to exogenous dsRNA and positive regulation of RIG-I signaling pathway), pro-inflammatory cytokine tumor necrosis factor (TNF) production, and antigen presenting cell (APC)

involvement (IL-27-mediated signaling pathway) (**Fig. 3d**). To confirm the upregulation of these pathways at a per-gene resolution in both infection models, heatmaps of the genes in the top 2 GO terms (positive regulation of IFN-β production and positive regulation of IκBK/NF-κB signaling) were made (**Fig. 3e**), with clear upregulation patterns in the infected mice vs. non-infected mice in both models, although the exact strength of upregulation and which genes were upregulated differed between the B6 Tg infection model relative to the CD-1 KI infection model. There was also remarkable homogeneity in expression profiles between mice within each infection model in these GO terms (**Fig. 3e**). Selected genes in pathogen recognition (*Ddx58* coding for RIG-I, a dsRNA sensor) and antiviral defenses (*Oas1a* involved in dsRNA cleavage and *Ly6e* that inhibits viral entry) were found to be upregulated in both B6 Tg inf. and CD-1 KI inf. versus their non-infected counterparts (**Fig. 3f**). Concordant down and discordant DEGs did not produce any significant GO terms. These GO term analyses provided an additional layer of evidence for similarities of host responses between the models involving the interferon and pathogen detection pathways but also some similarities in the pro-inflammatory and adaptive pathways.

GSEA-used as a complimentary approach to look at similarities between the models-was done using the GSEA_4.2.3 software from Broad Institute (Mootha et al., 2003; Subramanian, Tamayo, Mootha Vamsi, et al., 2005) using the C2.CP.Reactome.v7.5.1 gene sets and all gene's CPM matrix. Common gene sets having an FDR < 0.25 and normalized enrichment score (NES) > 1.5 were ranked according to highest average (of both CD-1 KI inf. and B6 Tg inf. comparisons) NES from which the top 25 were selected (**Fig. 4a**). The B6 Tg inf. comparison case had higher

weight in which gene sets were chosen as there was higher NES in most gene sets relative to the CD-1 KI inf. comparison case. Despite all these gene sets being common in both infected models, many of the top gene sets had quite higher NES in the B6 Tg mice (e.g.: IL-10 signaling NES of 1.55 compared to 4.22, IFN-γ signaling NES of 2.45 compared to 4.61, IFN-α/β signaling NES of 2.77 compared to 4.65, antigen processing cross presentation NES of 1.93 compared to 2.74, and receptor-interacting protein (RIP)-mediated NF-κB activation via Z-DNA-binding protein 1 (ZBP1) NES of 1.75 compared to 2.69 in CD-1 KI infection compared to B6 Tg infection, respectively) (**Fig. 4a**). There were gene sets upregulated during both infections in CD-1 KI and B6 Tg with similar NES involved in the cell cycle regulation and DNA replication (e.g.: G2-M checkpoints, origin recognition complex (ORC) 1 (ORC1) removal from chromatin, and activation of the pre-replicative complex) (**Fig. 4a**).

While NES are a good indicator of enrichment of gene sets and by proxy different biological pathways, leading edge analysis (also in the GSEA_4.2.3 software from Broad Institute) allows for the identification of genes that frequently appears in multiple gene sets selected as a marker of genes driving different outcomes in the comparison cases under consideration (both infected models). Leading edge genes were filtered for those present in at least 4 gene sets or if there was a difference of presence in 3 gene sets between the CD-1 KI inf. and B6 Tg inf. (e.g.: for a given gene, 3 gene sets in CD-1 KI inf. and 0 gene sets in B6 Tg inf.) comparison cases (to identify model-unique genes), resulting in 25 genes (**Fig. 4b**). The CPM of these genes were verified to see whether the genes were truly differentially expressed in both infection models relative to WT and/or non-infected controls. *Stat1*, tripartite motif protein 25 (*Trim25*), *Isg15*, and *Irf7*, all genes

involved in interferon production and signaling, were found highly and significantly expressed in CD-1 KI inf. and B6 Tg inf. relative to WT and non-infected controls (**Fig. 4c**).

Altogether, multiple complimentary approaches (qPCR, GO terms, GSEA, leading edge analysis, and read counts from RNA-seq) confirms that multiple pathways mainly centering on type 1 interferon and pathogen recognition might be similarly activated in response to SARS-CoV-2 infection. Having first obtained an idea of the similarities between the host responses, the differences between the models were explored.

Unique wound healing and proliferative transcriptional signature during CD-1 KI infection whereas B6 Tg inf. mice have increased chemokine signaling and pro-inflammatory responses, and a unique innate response. Continuing the examination of leading edge genes from the top 25 common gene set, B6 Tg inf. mice uniquely and significantly expresses *Nfkb2*, a subunit of the NF-κB complex and a major signaling pathway linked to antiviral and pro-inflammatory pathways (Wirasinha et al., 2021), and protein tyrosine phosphatase non-receptor type (PTPN) 6 (*Ptpn6*), encoding for SHP1 and involved in the negative regulation of pro-inflammatory pathways (e.g. mediated by mitogen-activated protein kinase (MAPK) and NF-κB) and increased type 1 IFN production by TLR signaling (An et al., 2008; Kanwal et al., 2013) (**Fig. 4d**). On the other hand, many other genes, including the ones identified as leading edge uniquely in CD-1 KI inf. vs. non-inf. did not meet significance threshold, likely because the sample size of CD-1 KI non-infected mice is smaller (n=3) due to 2 samples failing RIN RNA quality threshold.

GO term analysis (using threshold criteria described for **Fig. 3d** analysis) was performed on the unique up and down (greater than 0 and less than 0 FC, respectively) DEGs in B6 Tg inf. vs. non-inf. mice and CD-1 KI inf. vs. non-inf. mice (**Fig. 5a**). As seen in **Fig. 3a**, there are nearly 10-fold more unique DEGs during B6 Tg infection (total 3371 DEGs) compared to CD-1 KI infection (total 381 DEGs) (**Fig. 5a**). This lends increased power to the B6 Tg inf. GO term analysis, where many of the unique terms concern pro-inflammatory (i.e.: positive regulation of IL-6 production, positive regulation of TNF production, positive regulation IL-1β production, and positive regulation of IL-8 production) and adaptive response initiation (i.e.: positive regulation of T cell activation, positive regulation of phagocytosis, neutrophil chemotaxis, and antigen processing and presentation of exogenous peptide antigen via MHC class II) pathways (**Fig. 5c**). Downregulated GOs include cell fate canonical Wnt signaling GO term and positive transcription GO term (**Fig. 5c**), perhaps hinting at downregulation of regular cell processes during infection in the B6 Tg inf. mice. Meanwhile, CD-1 significant up GO terms only include cardiac GO terms (i.e.: cardiac muscle cell development and sarcomere organization) and down GO term sphingosine-1-phosphate signaling (**Fig. 5b**). To confirm the activation of these GO terms at a per-gene resolution, heatmap analysis was performed and revealed increased cardiac GO term genes' expression in the CD-1 KI inf. relative to non-inf. mice (**Fig. 5d**). The uniqueness of this upregulation pattern was confirmed as the same could not be said for B6 Tg inf. mice that have a more muddled expression profile for these cardiac GO terms (**Fig. 5d**). Similarly, looking at one of the top unique pro-inflammatory GO terms in the B6 Tg infection model, positive regulation of IL-6 production, (**Fig. 5e**) the expression profile is starkly upregulated in the

B6 Tg inf. relative to non-inf. mice, whereas the expression profile is mixed during CD-1 KI infection. In addition, top genes in the unique B6 Tg infection GO term positive regulation of T cell activation, are found to be uniquely and significantly upregulated during B6 Tg infection (**Fig. 5f**), including *B2m* (involved in antigen presentation and a component of major histocompatibility complex (MHC) complex (Li et al., 2016)), signal regulatory protein (SIRP) 1c (*Sirpb1c*) (belongs to a family of proteins involved in both positive regulation of T cell activation and phagocytosis (Hayashi et al., 2004; Lahoud et al., 2006)), and lymphocyte-specific protein tyrosine kinase (*Lck*) (involved in TCR signaling (Palacios & Weiss, 2004; Rossy et al., 2012)).

In addition, GSEA analysis (Mootha et al., 2003; Subramanian, Tamayo, Mootha, et al., 2005) identified unique gene sets selected based on uniquely significant (FDR < 0.25) up or down (positive or negative NES, respectively) gene sets or discordant gene sets (opposite NES sign of gene sets between models). In each infection model, both the top 7 up and down (by highest absolute value of NES) and 7 discordant gene sets were selected for analysis (**Fig. 6a-b**). CD-1 KI inf. mice have enriched gene sets involved in DNA replication and cell cycle progression (e.g.: DNA replication pre-initiation and mitotic G1 phase and G1/S transition) (**Fig. 6a**). Also, there are down in CD-1 KI inf. coagulation-related gene sets (e.g.: formation of fibrin clot/clotting cascade), hinting at anticoagulation induction in these mice (**Fig. 6a**).

Here, discordant down in CD-1 KI inf. mice and up in B6 KI inf. mice gene sets include guanine nucleotide-binding protein-coupled receptor (GPCR) signaling gene sets (e.g.: G alpha I signaling events and GPCR ligand binding) and T cell activation signaling gene sets (e.g.: generation of second messenger molecules, glycoprotein VI (GPVI)-

mediated activation cascade, and co-stimulation by the CD28 family) (**Fig. 6a-b**). Furthermore, B6 Tg inf. mice. uniquely have increased enrichment of the immunoregulatory interactions between a lymphoid and non-lymphoid cell gene set (NES 4.41) and multiple chemokine and cytokine signaling gene sets (e.g.: chemokine receptors bind chemokine and IL-4 and IL-13 signaling) (**Fig. 6b**). All these uniquely enriched gene sets in B6 Tg inf. mice might reflect a comparatively (to CD-1 KI inf. mice) increased innate-adaptive crosstalk (antigen presentation and chemokine and cytokine production and signaling) and adaptive response (T cell signaling), reflecting increased disease severity, a mounting viral response, and an inability to clear virus at 2 dpi. Enriched in non-inf. B6 Tg in comparison to inf. B6 Tg are cell structural gene sets (e.g.: cell-cell junction organization and laminin interactions) (**Fig. 6b**) might perhaps be due to increased entry of immune cells in the lungs and the consequential structural modifications during migration to reach infection sites but more likely due to disease associated destruction of structural tissues in the lungs.

Leading edge analysis was done for the 21 gene sets displayed in **Fig 6a-b** and filtered for genes in at least 4 gene sets (full list in **Supplementary Fig. 4**). Unique with increased expression genes in CD-1 KI inf. vs. non-inf. mice (and CD-1 WT inf. vs. non-inf. mice for all except *Prim1*) are a diverse list of genes including Cyclin A2 (*Ccna2*), proteasome 20S subunit alpha 4 (*Psma4*), minichromosome maintenance complex component 4 (*Mcm4*) (also down in B6 Tg inf. vs. non-inf.), and DNA primase subunit 1 (*Prim1*) (**Fig. 6c**). The upregulated expression of these genes in both KI and WT CD-1 inf. vs. non-inf. mice hints towards a unique infection response signature that may be mouse strain CD-1-specific.

Several chemokines and chemokine receptors are uniquely upregulated in response to B6 Tg infection including C-C chemokine ligand (CCL) 5 (*Ccl5*), *Ccr5*, *Cxcl16*, and *Ccr2* (**Fig. 6d**), indicating that the B6 Tg infection might cross a threshold of viral load or immune response activation that warrants increased involvement of different leukocytes to the cite of infection (lungs). Curiously, 2 genes (*Orc4* and 26S proteasome non-ATPase regulatory subunit 10 (*Psmd10*)) found to be uniquely present in CD-1 KI infection gene sets were not significantly increased or decreased in CD-1 KI mice but was found to be decreased during B6 Tg infection (**Fig. 6e**). As mentioned previously, many other genes, including the ones identified as leading edge uniquely in CD-1 KI inf. vs. non-inf. did not meet significance threshold, likely because the sample size of CD-1 KI non-infected mice is smaller (n=3), or because of redundancy of common gene sets, inflating the leading edge gene set number score of such genes.

Altogether, GO term analysis, GSEA, and leading edge analysis revealed differences in the host responses during infection at 2 dpi in the lungs between the 2 models. These differences were verified by looking at relative expression of genes and to identify a unique transcriptomic signature during CD-1 KI infection and a broad and fuller innate and adaptive immune activation during B6 Tg infection.

SARS-CoV-2 expression correlates with a T cell response during CD-1 KI infection and negatively correlates with intracellular transport networks during B6 Tg infection. As discussed earlier, there is a higher viral load in the lungs of B6 Tg inf. mice relative to CD-1 KI inf. mice at 2 dpi (as determined by PFU/g lung (**Fig. 1c**) and relative expression of viral nucleocapsid gene by qPCR (**Fig. 1d**)). Alignment of viral reads to

various genomic regions including spike, nucleocapsid, ORF7a, and RdRp (**Fig. 7a**), and CPM quantification of different viral regions (top **Fig. 7b**) confirms these earlier findings. However, when looking at proportion of SARS-CoV-2 reads aligned to different viral regions spike, nucleocapsid, ORF7a, and RdRp (**Fig. 7a**), the distribution of reads across those segments appear remarkably similar in both CD-1 KI inf. and B6 Tg inf. mice. Furthermore, the ratios of different gene segments appear remarkably consistent in both CD-1 KI inf. and B6 Tg inf. mice (bottom **Fig. 7b**). Both of these are a reassuring indication that SARS-CoV-2 replication is indeed occurring in both infected model and in a similar manner, because relative proportion of viral genomic segments are important for coronavirus fitness (Hartenian et al., 2020).

Certain insights can also be determined by looking at SARS-CoV-2 viral reads especially when viral reads are used as a proxy for abundance of viral load at a per sample basis. Since magnitude of viral reads are hugely different between models and suspecting that the dynamics of viral abundance and host response are different in the two models, Pearson correlations were separately calculated for CD-1 KI inf. and B6 Tg inf. mice between all detected host gene expression (CPM > 5 in 5 samples) and different viral genomic regions with a significance threshold for Pearson correlation coefficients of p-value < 0.05. The abundance of different viral genomic regions (in CPM) correlates strongly between each other (not shown) and, within each model's infection, there exists a perfect correlation of different viral genes' reads to any given host response gene (**Supplementary Fig. 5a-b**). For example, if nucleocapsid gene expression correlates positively with IRF7 gene expression in the B6 Tg inf. model, all the other viral genes must do so too.

The Pearson correlations for genes that were significantly correlated in both models were plotted (**Fig. 8a**) to bin genes into concordance/discordance categories (**Fig. 8a-b**). Genes uniquely positively and negatively correlated in each model were also determined; a remarkably high number of host genes (3916) correlated negatively with viral gene expression in the B6 Tg inf. mice while there were more positive correlated (614) compared to negatively correlated (318) host genes in the CD-1 KI inf. mice (**Fig. 8b**).

Entering gene sets for GO term analysis revealed a positive correlation of various T cell signaling GO terms (e.g.: TCR signaling pathway and positive regulation of IFN-γ production), hinting towards a balanced virus level-dependent T cell activation due either to lower viral levels (and hence below threshold for viral protein host response antagonism) or strain-specific differences. On the other hand, many negatively correlated genes are significantly associated with intracellular transport GO terms (e.g.: ER to Golgi vesicle-mediated transport, autophagosome assembly, cargo loading into coated protein complex II (COPII)-coated vesicles, and endosome to lysosome transport), indicating disruption of cellular transport networks. Other gene set categories did not achieve significance (FDR > 0.05).

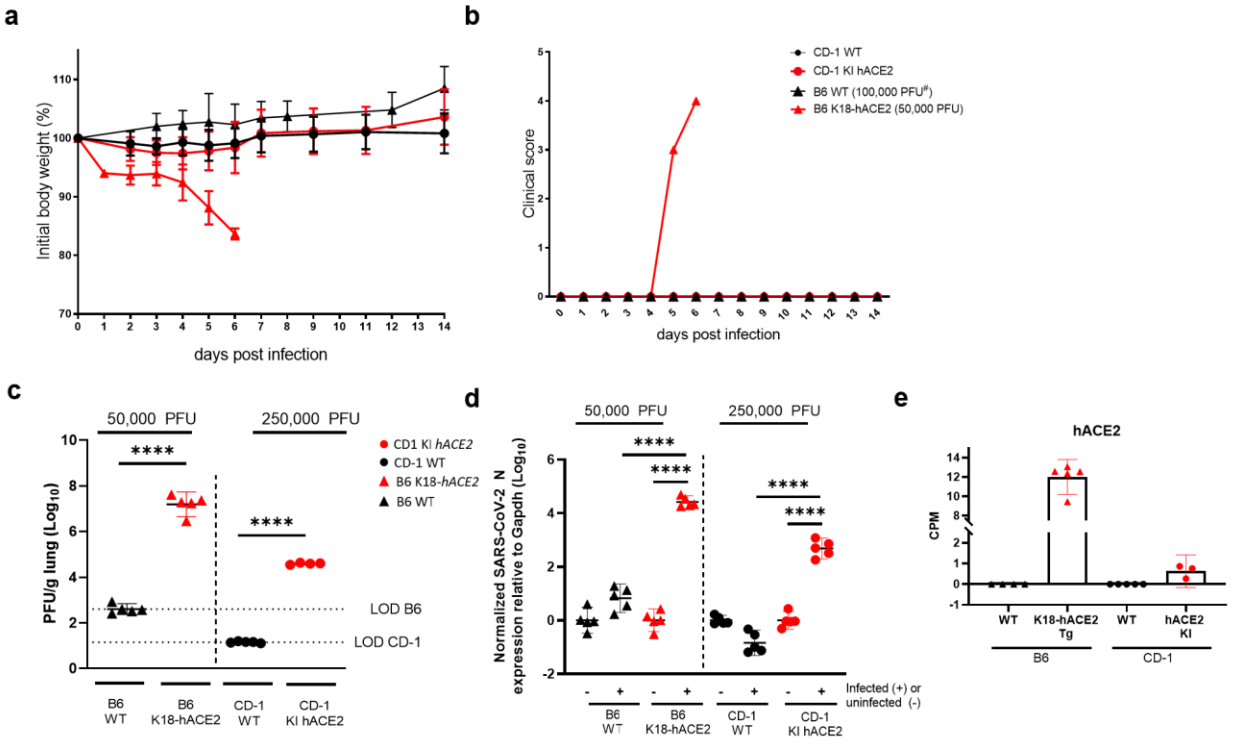

Figure 1. The CD-1 KI *hACE2* mouse model presents as an asymptomatic model of infection. Please see **Supplementary Fig. 1** for experimental details. #Note, for **a-b** survival experiment exclusively, B6 WT mice received 100,000 PFU compared to all other experiments and graphs presented in this thesis where they received 50,000 PFU. **a**, Percent body weight loss relative to day 0 (100%) measurements are shown for the survival experiment that lasted up to 14 days (experimental endpoint). **b**, Clinical score (as defined in **Supplementary Table 1**) was monitored throughout the course of infection. **c**, viral titers for infected mice only reported as $\log_{10}$(plaque forming units (PFU) per gram of lung). Separate limit of detections (LODs) were reported due to different lowest dilutions for B6 mice (10-fold) and CD-1 mice (2-fold). Data are presented as mean +/- 95% confidence interval (CI), n=5 per group (except n=4 for CD-1 Tg inf. group due to 1 outlier). p*<0.05, p**<0.01, p***<0.001, p****<0.0001 when WT inf. to Tg or KI inf. (for B6 and CD-1, respectively) groups are compared directly with unpaired-t test when number

of mice (n) per group are equal and normality condition has passed or Welch's t test when number of mice per group are unequal and normality condition has passed. **d**, relative quantification of SARS-CoV-2 nucleocapsid (N) gene expression reported as log_{10}(delta-delta cycle threshold (ddCt)) values are presented (normalized to *Gapdh* and respective to uninfected control groups). Gene expression undetected by cycle 40 was censored to 35.5 (lowest viral N cycle threshold in un-infected group). Data are presented as mean +/- 95% CI, n=5 per group. p*<0.05, p**<0.01, p***<0.001, p****<0.0001 using one-way ANOVA test with Tukey's test for multiple comparisons. **e**, CPM of *hACE2* are presented for un-infected B6 and CD-1 WT as well as B6 Tg and CD-1 KI mice. Data are presented as mean +/- 95% CI, n=5 per group (except for (**e**) where n=4 for B6 WT non-inf. and n=3 for CD-1 KI non-inf.).

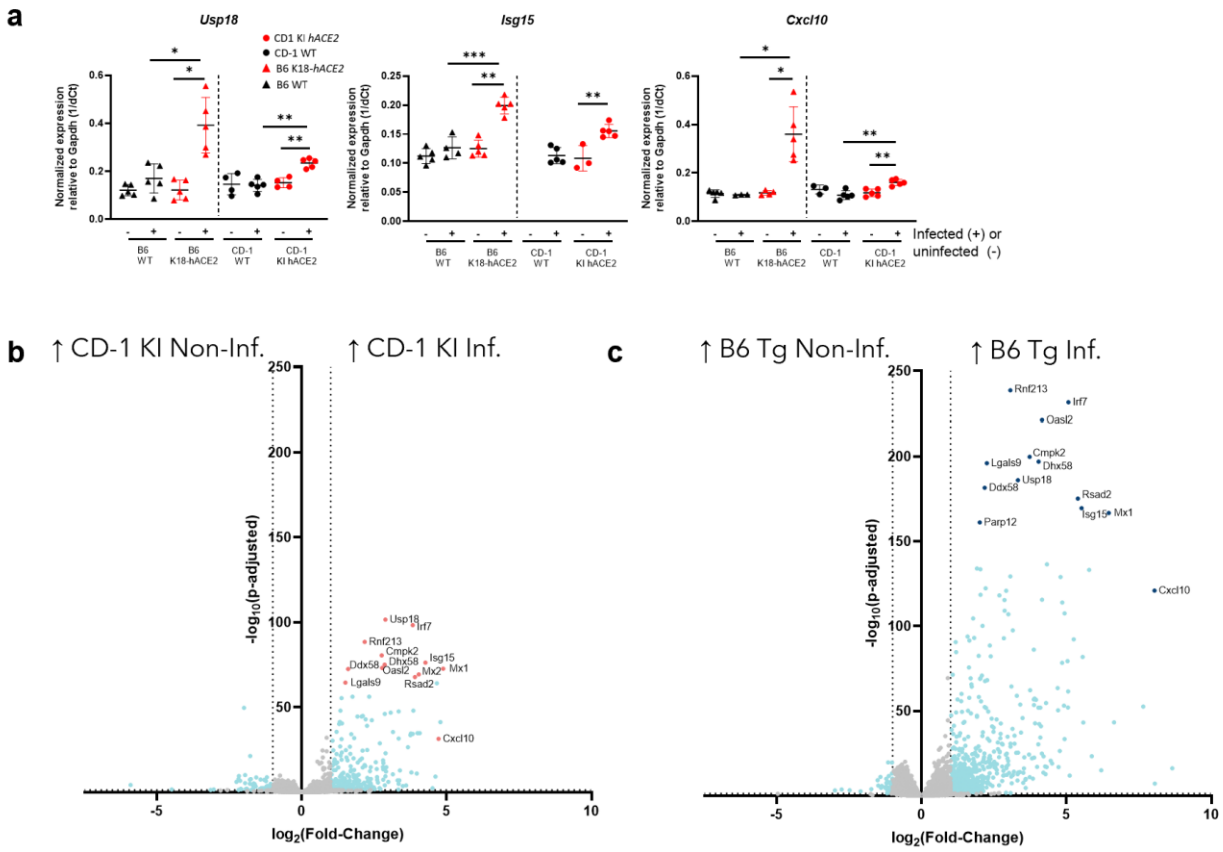

Figure 2. Similar top hits seen in host responses of both CD-1 KI and B6 Tg infected mice. a, Please see **Supplementary Fig. 1** for experimental details. Relative expression in lungs at 2 dpi for genes *Isg15*, *Usp18*, and *Cxcl10* are presented as 1/delta cycle threshold (dCt) values (normalized to *Gapdh*). Data are presented as mean +/- SD, n=5 per group. Undetected reactions by cycle 40 were not used for calculations. p*<0.05, p**<0.01, p***<0.001, p****<0.0001 using Brown-Forsythe's one-way ANOVA test with Dunnett's T3 multiple comparison test. **b-c**, Differentially expressed genes (DEGs) determined using DESeq2 (Love et al., 2014) were compared for (**b**) CD-1 KI inf. vs. non-inf. and (**c**) B6 Tg inf. vs. non-inf. mice. The right and left side of both graphs denotes infected and non-infected groups, respectively. DEGs were defined as those having an adjusted p-value of less than 0.05 after an initial gene detection threshold of greater than

5 CPM in 5 samples. An additional graphing threshold of above absolute value of 1.0 log2(fold-change) was chosen to look at largely up and down-regulated genes in this figure exclusively. Top 13 (ranked by significance) DEGs are displayed in dark blue and orange for B6 Tg inf. vs. non-inf. (**c**) and CD-1 KI inf. vs. non-inf. (**b**), respectively. Light blue denotes the DEGs with the fold-change threshold.

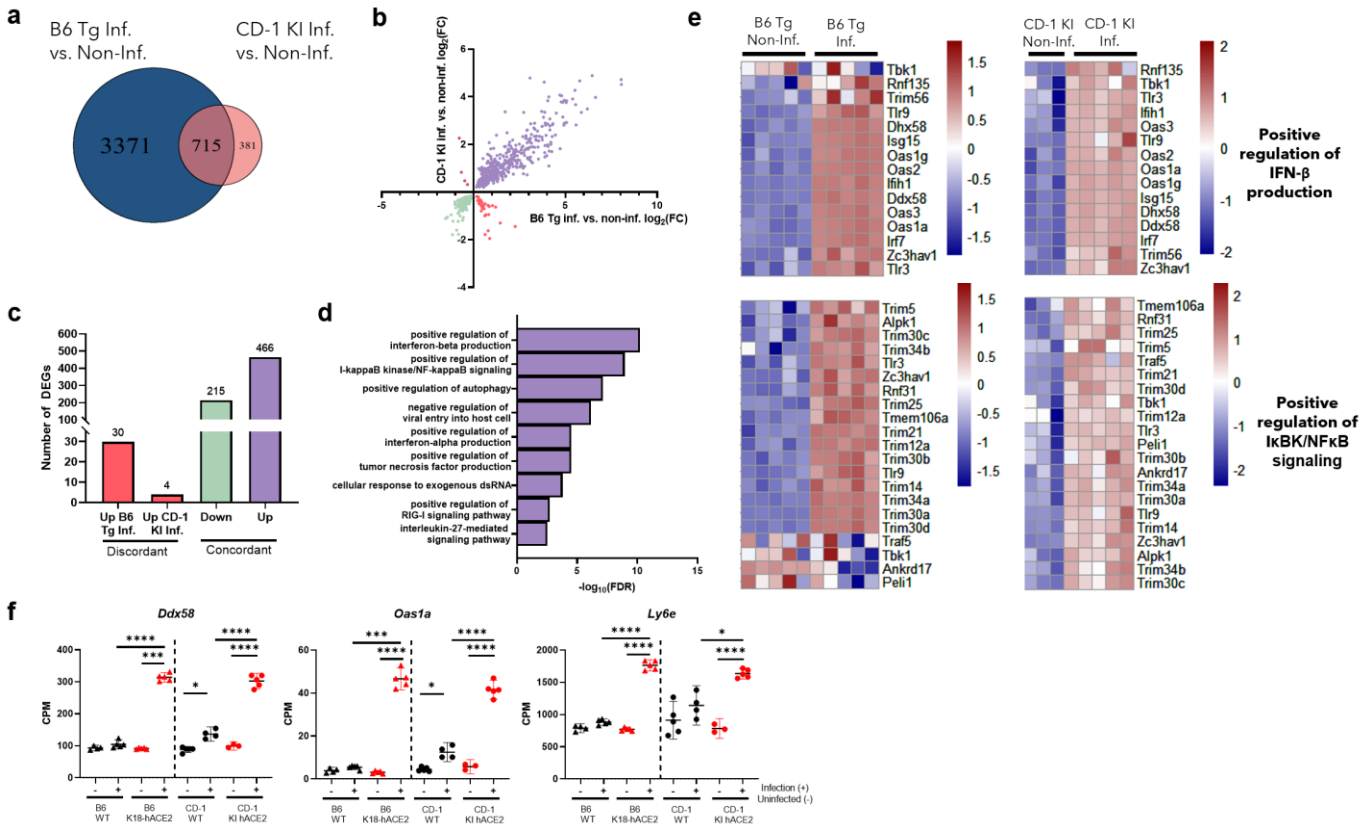

Figure 3. Concordant early immunity and upregulated pathogen detection gene expression modules in both CD-1 KI and B6 Tg infected mice. a, Number of DEGs uniquely in the B6 Tg comparison case and CD-1 KI comparison case as well as common DEGs (less than 0.05 adjusted p-value). DEGs are considered unique if they are present (passed significance threshold) in the list of one comparison case and absent (did not pass significance threshold) in the second comparison case. **b**, Concordant/discordant analysis looking at the log2(fold-change) of common DEGs (B6 Tg inf. vs. non-inf. on the x-axis, CD-1 KI inf. vs. non-inf. on the y-axis). **c**, Count of DEGs in the different concordant/discordant categories. **d**, BP GO terms are displayed for the concordant upregulated genes (fold-change > 0 and adjusted p-value < 0.05) and were calculated using the DAVID software (Huang da et al., 2009; Sherman et al., 2022). Only GO terms with at least one parent hierarchy tree of level 8 or greater were considered to filter for

biologically specific GO terms and with an FDR value cut-off of 0.05. **e**, Heatmap of (left) B6 Tg non-inf. and B6 Tg inf. mice and (right) CD-1 KI non-inf. and CD-1 KI inf. mice of genes found in the GO terms (top) positive regulation of IFN-β production and (bottom) positive regulation of IκBK/NF-κB signaling. Log_{10}(CPM) values are Z-normalized within each comparison case, with the Z-score scale shown besides each heatmap. **f**, CPM of select example genes involved in pathogen recognition (*Ddx58*), antiviral response (*Oas1a* and *Ly6e*). Data are presented as mean +/- 95% CI, n=5 per group (except n=4 for B6 WT non-inf., n=4 for D-1 WT inf., and n=3 for CD-1 KI non-inf.). p*<0.05, p**<0.01, p***<0.001, p****<0.0001 using Brown-Forsythe's one-way ANOVA test with Dunnett's T3 multiple comparison test.

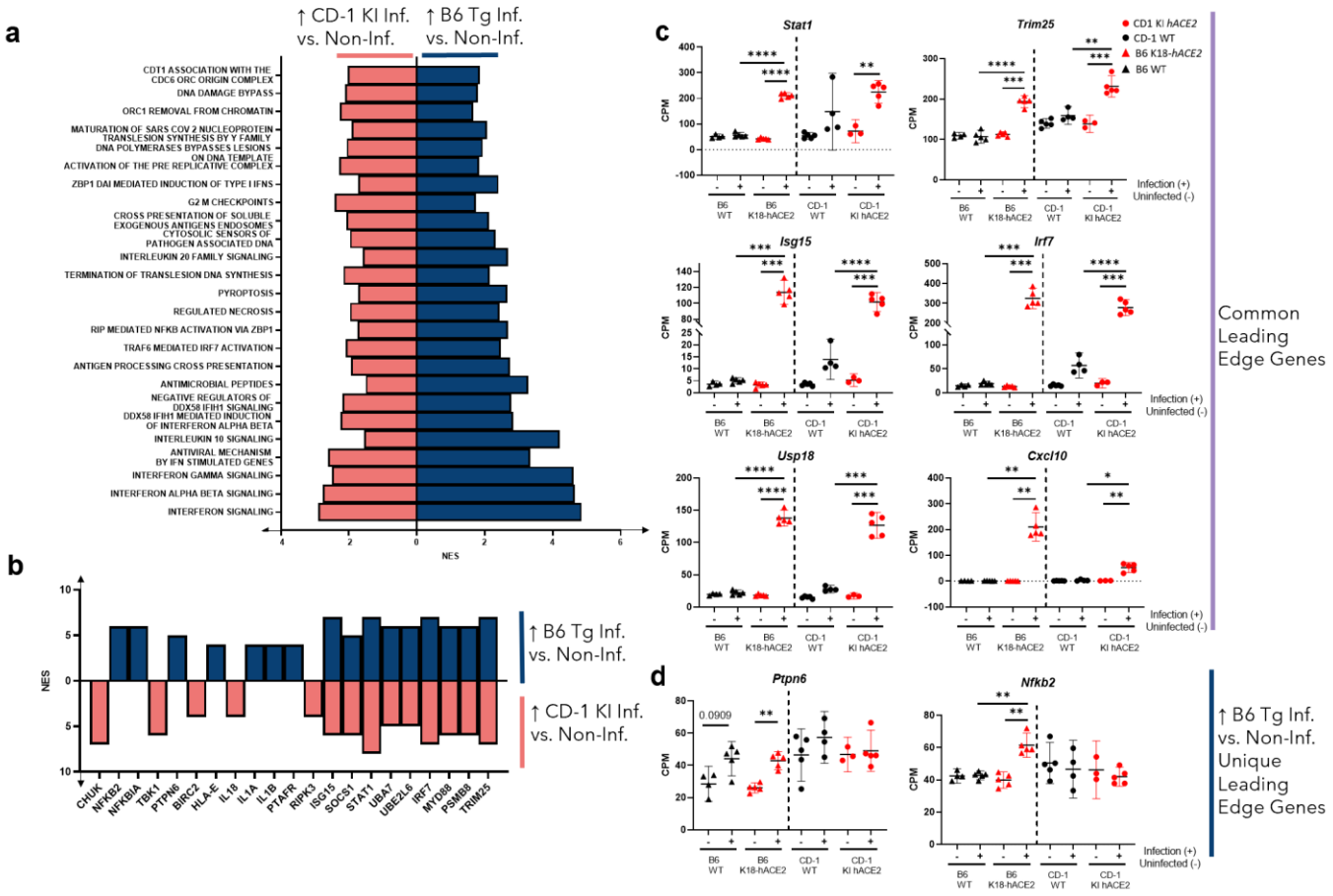

Figure 4. Unique type 1 IFN pathway signaling during B6 Tg infection despite similarities with CD-1 KI infection. a-b, Gene set enrichment analysis using GSEA_4.2.3 software from Broad Institute (Mootha et al., 2003; Subramanian, Tamayo, Mootha Vamsi, et al., 2005) using the C2.CP.Reactome.v7.5.1 gene sets and all gene's CPM matrix. Common gene sets having an FDR < 0.25 and NES > 1.5 were ranked according to highest average (of both CD-1 KI and B6 Tg inf.) NES from which the top 25 were selected. (**a**) NES for gene sets upregulated in CD-1 KI inf. vs. non-inf. are shown in orange and upregulated gene sets in B6 Tg inf. vs. non-inf. are shown in dark blue. (**b**) Leading edge analysis was done for the genes appearing in the most sets for both CD-1 KI inf. and B6 Tg inf. mice, considering a threshold of either 4 or a difference between

CD-1 KI inf. and B6 Tg inf. of 3. Y-axis displays number of gene sets each gene is found in. **c-d**, Notable CPM of leading edge genes are displayed for (**c**) common leading edge genes and (**d**) unique up in B6 Tg inf. genes. Data are presented as mean +/- 95% CI, n=5 per group (except n=4 for B6 WT non-inf., n=4 for D-1 WT inf., and n=3 for CD-1 KI non-inf.). p*<0.05, p**<0.01, p***<0.001, p****<0.0001 using Brown-Forsythe's one-way ANOVA test with Dunnett's T3 multiple comparison test.

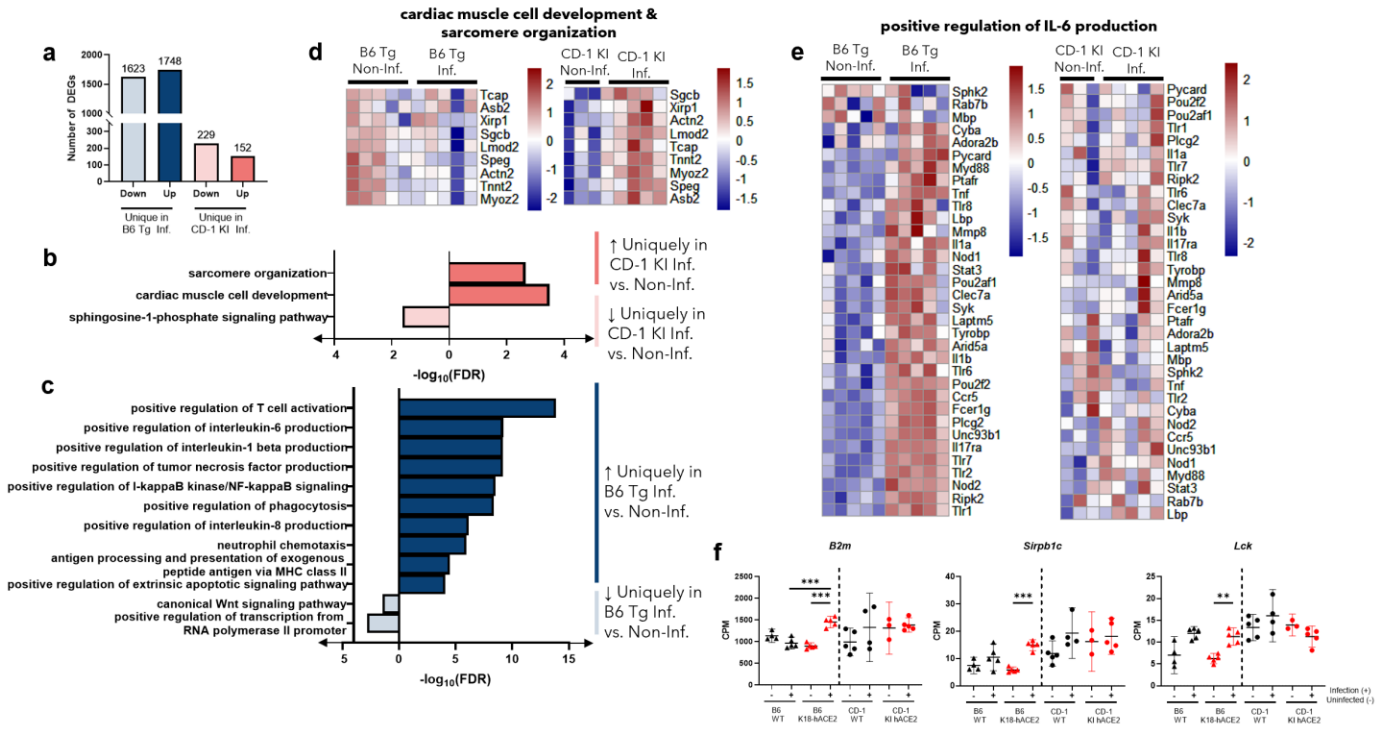

Figure 5: B6 Tg infection uniquely unleashes pro-inflammatory and early antigen presentation modules. a, Count of DEGs in the uniquely up or down during B6 Tg or CD-1 KI infection. **b-c**, BP GO terms are displayed for uniquely up (FC > 0) or down (FC < 0) in CD-1 KI infection and B6 Tg infection (all for adjusted p-value < 0.05) and were calculated using the DAVID software (Huang da et al., 2009; Sherman et al., 2022). Only GO terms with at least one parent hierarchy tree of level 8 or greater were considered to filter for biologically specific GO terms and with an FDR value cut-off of 0.05. GO terms uniquely (**b**) up (bright orange) and down (light orange) during CD-1 KI infection and (**c**) up (dark blue) and down (light blue) during B6 Tg infection are displayed with -$\log_{10}$(FDR) values. **d-e**, Heatmap of (left) B6 Tg non-inf. and B6 Tg inf. mice and (right) CD-1 KI non-inf. and CD-1 KI inf. mice of genes found in the GO terms (**d**) cardiac muscle cell development and sarcomere organization, and (**e**) positive regulation of IL-6 production. Log_{10}(CPM) values are Z-normalized within each comparison case, with the Z-score scale

shown besides each heatmap. **f**, CPM of select example genes in the positive regulation of T cell activation GO term. Data are presented as mean +/- 95% CI, n=5 per group (except n=4 for B6 WT non-inf., n=4 for D-1 WT inf., and n=3 for CD-1 KI non-inf.). p*<0.05, p**<0.01, p***<0.001, p****<0.0001 using Brown-Forsythe's one-way ANOVA test with Dunnett's T3 multiple comparison test.

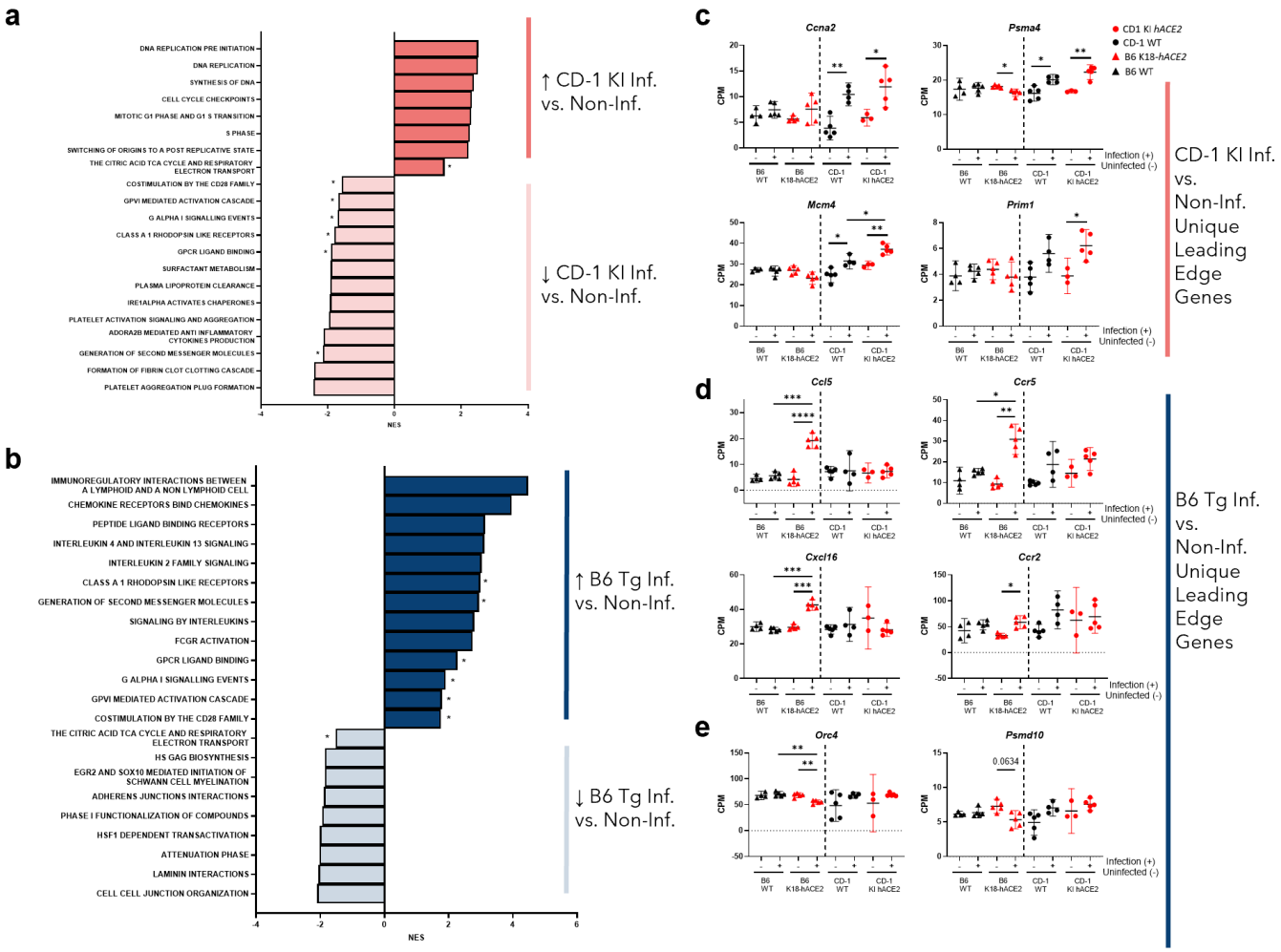

Figure 6. Unique CD-1 KI infection wound healing signature whereas a unique chemokine and chemokine receptors signature during B6 Tg infection. **a-b**, Gene set enrichment analysis using GSEA_4.2.3 software from Broad Institute (Mootha et al., 2003; Subramanian, Tamayo, Mootha Vamsi, et al., 2005) using the C2.CP.Reactome.v7.5.1 gene sets and all gene's CPM matrix. Unique or discordant gene sets having an FDR < 0.25 and NES > 1.5 were ranked according to NES from which the top 7 highest NES, 7 lowest NES, and 7 discordant gene sets were chosen. NES for gene sets (**a**) up (bright orange) and down (light orange) during CD-1 KI infection and (**b**) up (dark blue) and down (light blue) during B6 Tg infection. * denotes discordant gene sets

(up in one mouse model while down in the other. **c-e**, Notable CPM of leading edge genes (full list in **Supplementary Fig. 4**) are displayed for (**c**) unique up in CD-1 KI inf. genes and (**d**) unique up in B6 Tg inf. genes, and (**e**) unique down in B6 Tg inf. genes. Data are presented as mean +/- 95% CI, n=5 per group (except n=4 for B6 WT non-inf., n=4 for D-1 WT inf., and n=3 for CD-1 KI non-inf.). p*<0.05, p**<0.01, p***<0.001, p****<0.0001 using Brown-Forsythe's one-way ANOVA test with Dunnett's T3 multiple comparison test.

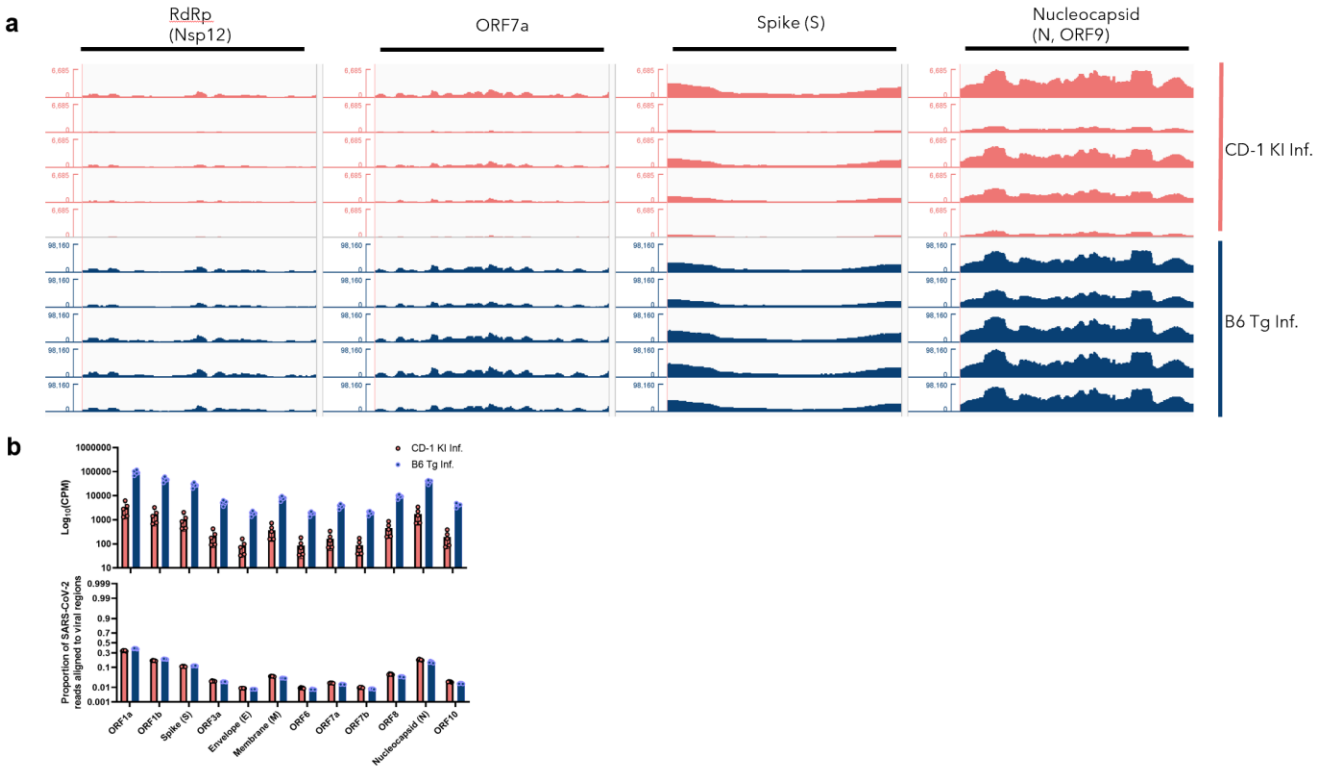

Figure 7. Similar proportion of viral reads in CD-1 KI infected mice despite lower viral amounts compared to B6 Tg infected mice. a, Viral reads mapping to viral genome regions of RdRp (Nsp12), ORF7a, spike (S), and nucleocapsid (N or ORF9) visualized with the IGV software (Robinson et al., 2017; Robinson et al., 2011; Thorvaldsdóttir et al., 2012) for all 5 mice in each of CD-1 KI inf. and B6 Tg inf. groups. **b**, (Top) $\log_{10}$(CPM) of viral reads for different viral genomic regions and (bottom) proportion of SARS-CoV-2 viral reads aligned to different viral regions.

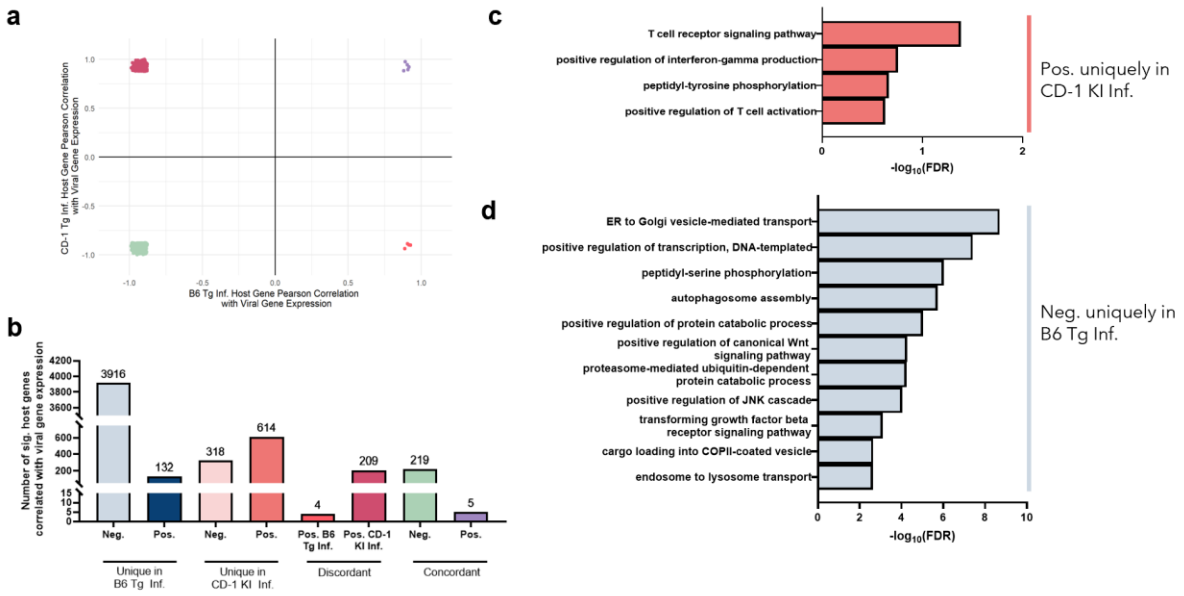

Figure 8. Viral gene expression correlates with T cell response during CD-1 KI infection whereas there is a negative correlation of viral expression with intracellular transport networks in B6 Tg infection. a, Concordance/discordance of Pearson correlation coefficients of common host genes (437) in B6 Tg inf. and CD-1 KI inf. mice having a significant correlation (chosen at $p<0.05$) with different viral genes (averaged all viral gene expression's coefficients as all viral genes' expression are perfectly concordant as shown in **Supplementary Fig. 5**). X-axis and y-axis maps Pearson correlation coefficients of B6 Tg inf. and CD-1 KI inf. mice, respectively, to viral gene expression. **b**, Count of host genes in the different concordant/discordant and unique positive and negative Pearson correlation coefficients to viral genes in CD-1 KI inf. and B6 Tg inf. mice. **c-d**, BP GO terms are displayed for the significantly correlated genes (p-value < 0.05) in the different categories and were calculated using the DAVID software (Huang da et al., 2009; Sherman et al., 2022). Only GO terms with at least one parent hierarchy tree of level 8 or greater were considered to filter for biologically specific GO terms and with an FDR value cut-off of 0.05. GO terms uniquely (**c**) up (bright orange)

during CD-1 KI infection and (**d**) down (light blue) during B6 Tg infection are displayed with -$\log_{10}$(FDR) values.

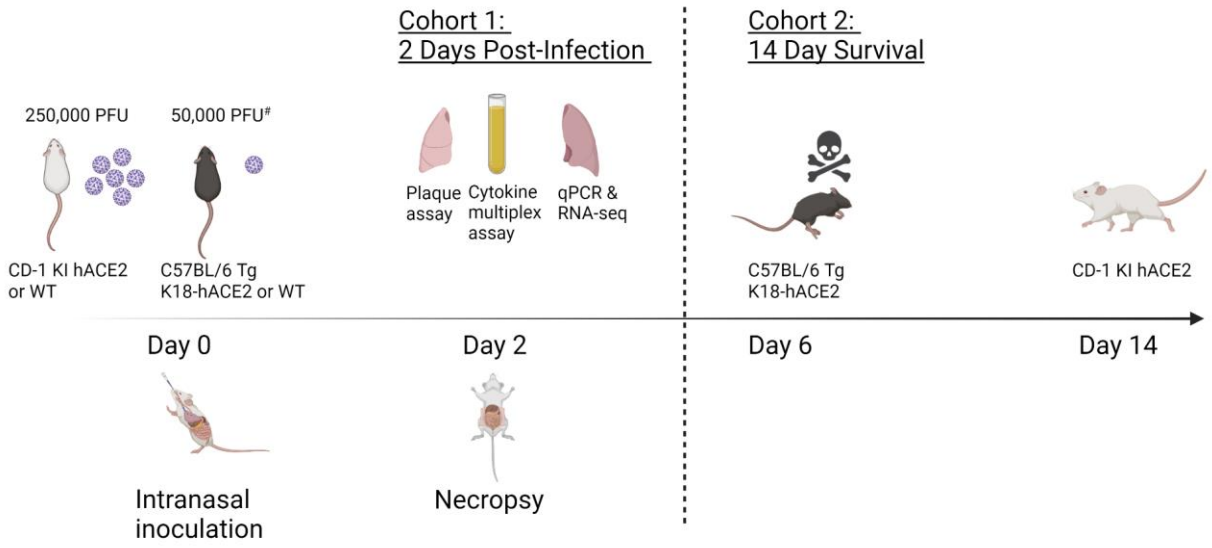

Supplementary Figure 1. Experimental design of infection and cohort separation. Male CD-1 *hACE2* KI hemizygous or WT (250,000 PFU) and male B6 K18-*hACE2* hemizygous transgenic or WT (50,000 PFU) were infected with SARS-CoV-2 IN or not-infected. #Note, for survival experiment exclusively, B6 WT mice received 100,000 PFU compared to all other experiments and graphs presented where they received 50,000 PFU.

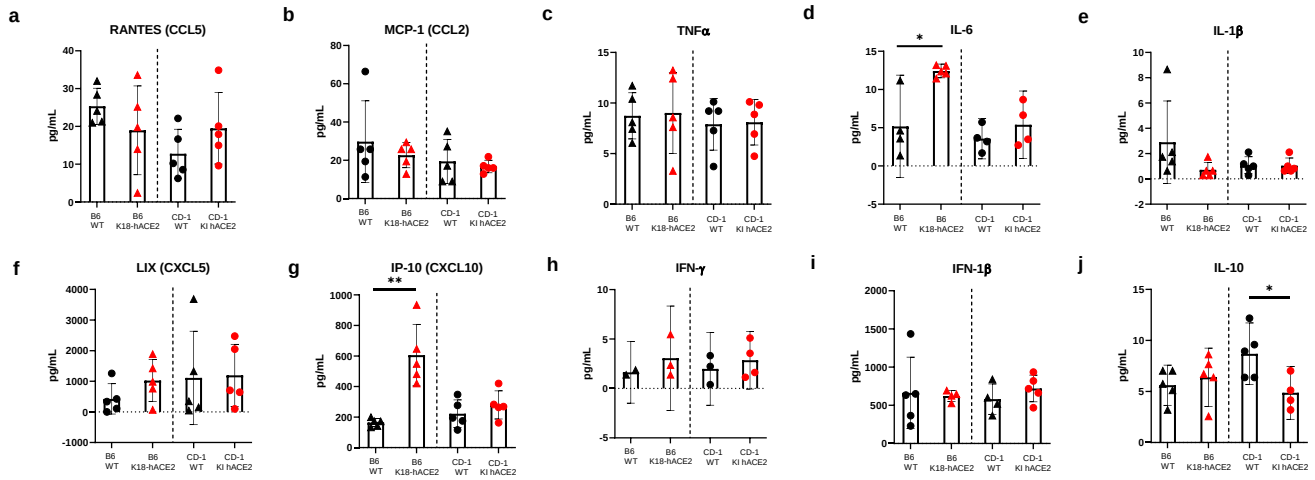

Supplementary Figure 2. Only CXCL10 (IP-10) and IL-6 protein is significantly up in plasma at 2 dpi in B6 Tg infected compared to B6 WT infected mice. a-j, Plasma cytokine protein expression as measured by the 44-multiplex cytokine measurement from Eves Technologies for (**a**) RANTES (CCL5), (**b**) MCP-1 (CCL2), (**c**) TNFα, (**d**) IL-6, (**e**) IL-1β, (**f**) LIX (CXCL5), (**g**) IP-10 (CXCL10), (**h**) IFN-γ, (**i**) IFN-1β, and (**j**) IL-10. p*<0.05, p**<0.01, p***<0.001, p****<0.0001 when WT inf. to Tg or KI inf. (for B6 and CD-1, respectively) groups are compared directly with unpaired-t test when number of mice (n) per group are equal and normality condition has passed or Welch's t test when number of mice per group are unequal and normality condition has passed.

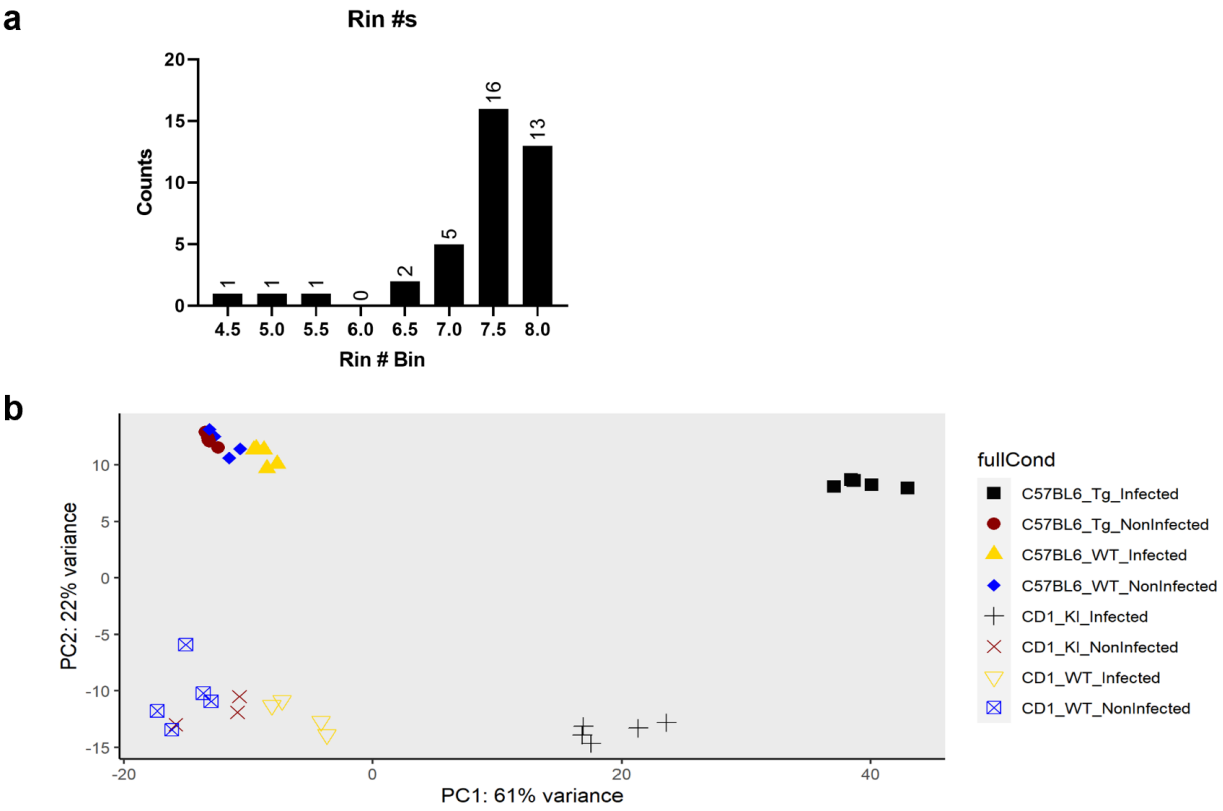

Supplementary Figure 3. Quality control for RNAseq sample generation and post-processing. a, RIN number distribution for 39 RNA samples sent for bioanalysis, 3 of which was rejected for very low RIN (under 6.0). **b**, PCA analysis demonstrating the clustering of samples based on PC1 (weighted for infection-specific genes) and PC2 (weighted for strain-specific genes).

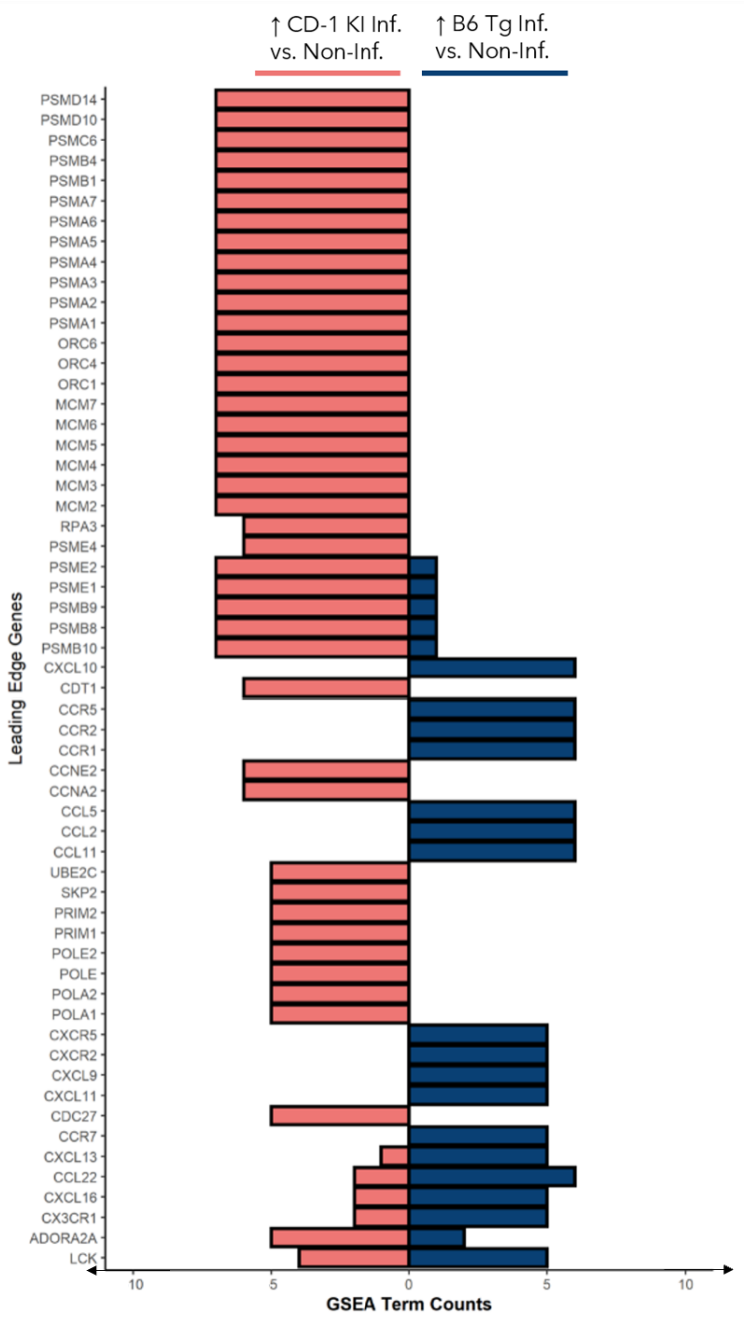

Supplementary Figure 4. Leading edge genes for unique or discordant gene sets. Leading edge genes for the combined 35 unique or discordant gene sets during B6 Tg and CD-1 KI infection as discussed in **Fig. 6a-b**. Thresholds were 4 gene sets in either model. Gene set numbers for genes unique or discordant during CD-1 KI infection (bright orange) and during B6 Tg infection (dark blue).

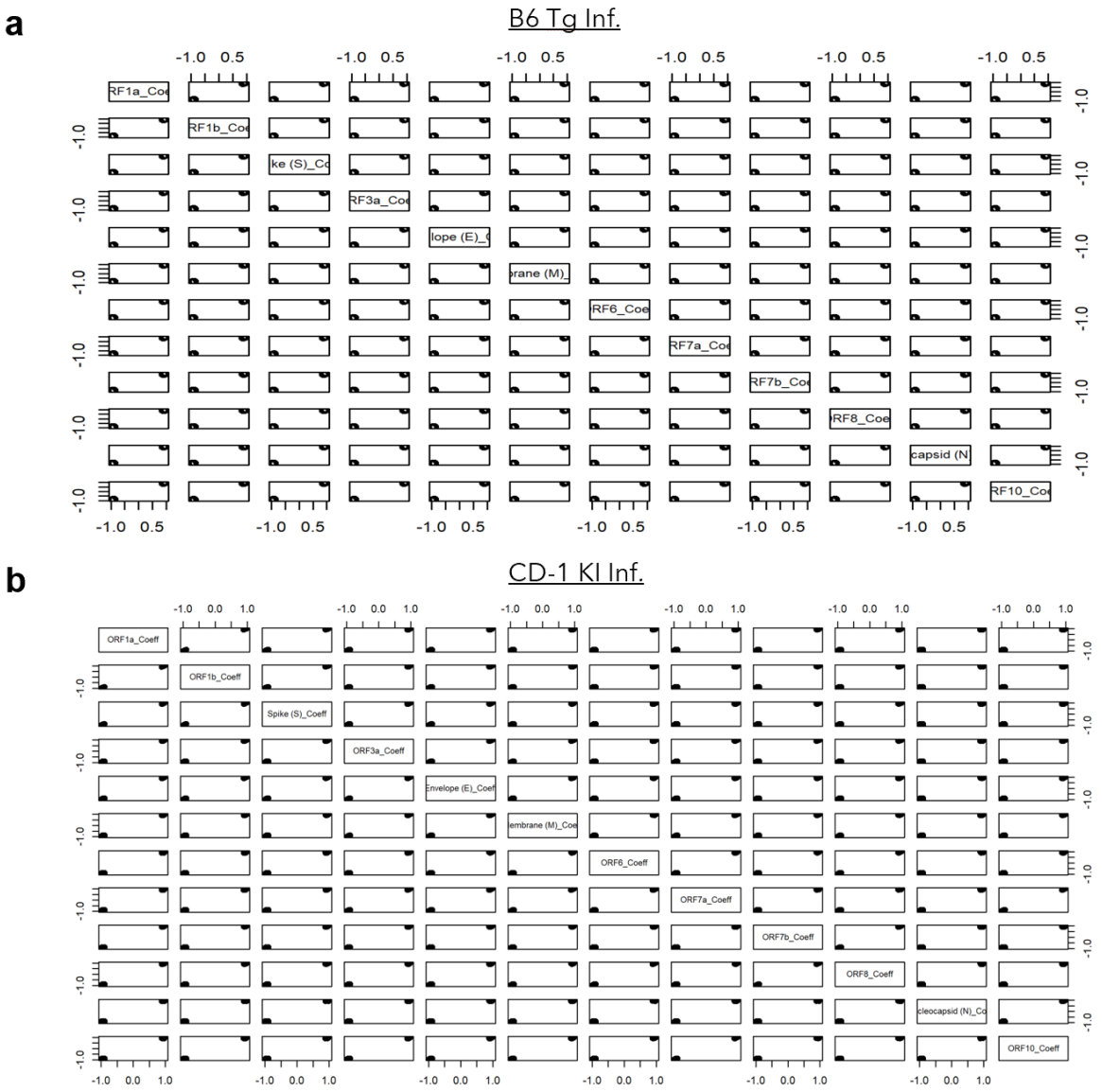

Supplementary Figure 5. Absolute concordance between all SARS-CoV-2's genes. **a-b**, Pair-wise mapping of significant ($p<0.05$) Pearson correlation coefficients between different SARS-CoV-2 and all host genes detected (CPM>5 in 5 samples) in (**a**) B6 Tg inf. mice (5 mice, 4485 genes past thresholds), and (**b**) CD-1 KI inf. mice (5 mice, 1369 host genes past thresholds).

General Clinical Scoring for Infections	
Clinical score	**Observation**
Score=0	Normal Behaviour AND Active AND No Aberrant Fur
Score=1	Piloerection AND/OR Mild Ruffled Fur
Score=2	Mild Hunched Posture OR Mild Ruffled Fur AND Slightly Less Active
Score=3	Mild Hunched Posture AND Mild Ruffled Fur AND Less Active
Score=4	Hunched Posture AND Ruffled Fur AND Inactive
Score=5	Death

Supplementary Table 1. **Clinical score guidelines.** Guidelines for scoring severity of infection and to guide humane euthanasia endpoint (or clinical endpoint). A score above 3 is considered sufficient criteria for euthanasia (or a loss of greater than 80% body weight since the start of the experiment).

Nucleotide Position	Nucleotide Change	Type of Mutation	Protein/UTR region	Amino acid Change
SARS-CoV-2 CP13.32 P4 passage 4				
241	C->T	extragenic SNP	5'UTR	NA
3037	C->T	SNP silent	NSP3	F106F
5422	T->C	SNP silent	NSP3	N901N
14408	C->T	SNP coding	NSP12b	P314L
15324	C->T	SNP silent	NSP12b	N619N
21784	T->A	SNP coding	S	N74K
23403	A->G	SNP coding	S	D614G
25433	C->T	SNP coding	ORF3a	T14I
SARS-CoV-2 CP13.32 P4 passage 2				
241	C->T	extragenic SNP	5'UTR	NA
3037	C->T	SNP silent	NSP3	F106F
5422	T->C	SNP silent	NSP3	N901N
14408	C->T	SNP coding	NSP12b	P314L
15324	C->T	SNP silent	NSP12b	N619N
23403	A->G	SNP coding	S	D614G
25433	C->T	SNP coding	ORF3a	T14I

Supplementary Table 2. **SARS-CoV-2 clinical isolate CP13.32 P4's consensus mutations and amino acid changes across passages.** List of all consensus mutations and amino acid changes in passage 4 (top) and 2 (bottom) for the CP13.32 P4 isolates relative to the Wuhan-Hu-1 NC_045512 sequence. Only mutations T21784A (coding for N74K in spike) arose from passage 2 to 4 (highlighted in light blue). SNP: single nucleotide polymorphism

Chapter 4: Discussion

The survival (no deaths during a 14-day survival), body weight change (no significant body weight changes), and clinical score (no signs or symptoms) data along with the presence of infectious viral particles at 2 dpi in the lungs suggests that the CD-1 KI model presents an asymptomatic infection course in comparison to the here validated B6 Tg severe disease model (previously characterized by Michael Diamond's lab (Winkler et al., 2020) and Vincent Munster's lab (Yinda et al., 2021)). This asymptomatic disease presentation occurs despite the 5-fold higher virus inoculum in the CD-1 KI mice (chosen due to data not shown from lower doses demonstrating little susceptibility of the KI model to infection evidenced by no infectious viral particles isolated at 2 dpi therein). Further exploration of symptoms, and functional and histological assessment of the lungs and other organs are warranted to cement the claim of the CD-1 KI mice being an asymptomatic model of SARS-CoV-2 infection.

At 2 dpi, the viral load in the lungs is much greater in the B6 Tg mice compared to the CD-1 KI. One possible explanation is the presence of strain-specific genetic susceptibility or protection factors during SARS-CoV-2 infection as seen for the type 1 helper T cell response skew in B6 mice compared to a type 2 helper T cell response skew in BALB/c, A/J, and DBA/2 mice, conferring increased resistance to *Leishmania major* infection in the B6 mice (Mills et al., 2000). Recently, a study used collaborative cross mice (a cross of several inbred strains bearing high genetic diversity (Threadgill et al., 2011)) in order to investigate different infection outcomes in response to SARS-CoV infection and thereby discovered that baseline T cell, specifically a dysregulated and pro-inflammatory signature, associates with severe disease upon infection (Graham et al.,

2021). A second explanation may be promoter strengths differences and/or differential cell-type protein expression patterns of hACE2 in both models allows for greater viral reproduction in B6 *hACE2* Tg. Indeed, many studies have shown the high expression of *hACE2* relative to *mAce2* in multiple tissues (Shuai et al., 2021; Winkler et al., 2020) in the B6 K18-*hACE2* model. Therefore, our CD-1 KI model wherein *hACE2* expression is driven by mouse promoter will also be weaker compared to *hACE2* expression in the B6 Tg mice as we also demonstrated by RNAseq counts. These differential *hACE2* expression patterns might also explain why the infection in the B6 K18-*hACE2* sometimes leads to encephalitis and neurological findings that might at least partially (but not fully) explain increased disease severity (Oladunni et al., 2020; Song et al., 2021; Winkler et al., 2020; Yinda et al., 2021).

The only significant plasma proteomic findings were CXCL10 and IL-6 being higher in the B6 Tg inf. vs. WT inf. mice, hinting that perhaps day 2 in the plasma is too early to notice protein-level changes of various other cytokines and chemokines that are expected to be upregulated throughout the course of infection for the B6 Tg inf. mice (Oladunni et al., 2020; Winkler et al., 2020; Yinda et al., 2021).

Lung RNA transcriptomics are a better tissue and sample type to assess early (2 dpi) host response changes in both models. By qPCR (and confirmed in RNA-seq), the significant increased expression relative to WT and non-inf. groups of *Cxcl10* (a chemokine for the recruitment of numerous immune cell types), *Isg15*, and *Usp18* (all three of which are ISGs) in the lungs suggested the presence of a host response. For broader transcriptomic assessment, RNA-seq was done. To control for strain-specific differences, transcriptomic analysis will only compare CD-1 KI inf. to non-inf. and B6 Tg

inf. to non-inf. At a first glance there are both a larger number of differentially expressed genes during B6 Tg infection compared to during the CD-1 KI infection as well as a higher fold-change and significance of many of the common DEGs, hinting towards a broader host response of higher magnitude in the B6 Tg inf. mice relative to the CD-1 KI inf. mice. Nevertheless, as expected from the preliminary qPCR findings, many interferon signaling, ISGs', and pathogen recognition GO terms and gene sets are commonly found in both CD-1 KI and B6 Tg models during infection. The validity of these GO terms are also confirmed by looking at a per-gene-basis at the genes in the positive regulation of IFN-β production and positive regulation of IκBK/NFκB signaling in inf. vs. non-inf. B6 Tg and CD-1 KI that both show stark upregulation across the spectrum. The identification of strong upregulation of *Irf7*, *Stat1*, *Isg15*, and *Trim25* in both models compared to WT and non-inf. groups validated the pathway-level findings for these aforementioned early innate immunity modules that was also previously demonstrated for the B6 Tg severe model (Oladunni et al., 2020; Winkler et al., 2020). Surprisingly (given the non-severe infection in the CD-1 KI inf. mice), GO terms and gene sets in the CD-1 KI inf. mice (also present in the B6 Tg inf. mice) also included pro-inflammatory cytokine production (e.g.: TNF) and antigen presentation terms.

Considering just these findings at face value and ignoring the model-specific differences discussed afterwards, several explanations may be given for why the disease outcomes are so different despite the similarities outlined. Concerning various pro-inflammatory pathways, several studies in humans, mice, and *in vitro* systems have suggested a pathological role (Darif et al., 2021; Karki et al., 2021; Neufeldt et al., 2022; Sefik et al., 2022). For the CD-1 KI inf. mice, the observation of an asymptomatic

phenotype despite the pro-inflammatory findings may indicate that either these pathways are indeed elicited in response to the virus and help directly in viral clearance in this model specifically, perhaps due to CD-1-strain specific reasons, or that these modules are bystander pathway activations that occur alongside the previously mentioned early innate immunity module composed of interferon signaling, interferon-stimulate gene networks, and pathogen recognition pathways that mainly clear the virus. An alternative or combining factor could be that the ease of virus multiplication in the B6 Tg mice with a huge abundance of hACE2 is harder for the immune system to get under control despite interferon signaling in these mice relative to the CD-1 KI mice wherein SARS-CoV-2 already has difficulty in sustaining replication due to scarcity of hACE2 expression and that the immune system herein easily combats the virus.

The next layer of evidence concerning model-specific host responses provides additional potential explanation for disease severity differences. The CD-1 KI inf. mice have uniquely downregulated clotting gene sets that might indicate direct viral anti-coagulation effects to counter coagulation's physiological role in limiting pathogen dissemination through the blood (Antoniak, 2018), however, such phenomenon were not found reported in the literature. Another explanation may be strain-specific coagulation pathway differences as reported in other mouse backgrounds (Kopić et al., 2019).

Additionally, several DNA replication and cell cycle gene sets as well as genes *Prim1*, encoding for a subunit of DNA primase (Parry et al., 2020), and *Mcm4* (also significantly down in B6 Tg inf. mice), involved in cell cycle progression and licensing of DNA replication (Das et al., 2015), are upregulated in the CD-1 KI inf. mice, perhaps due to a wound repair response specific to the CD-1 strain of mice. In support of such a

hypothesis, cardiac muscle GO terms are upregulated and *Ccn2A*, found to be induced in endocardial cells for repopulation of damaged tissues in a zebrafish heart injury model (Mukherjee et al., 2021), is uniquely upregulated in both the CD-1 KI inf. vs. non-inf. and CD-1 WT inf. vs. non-inf. mice (same pattern also seen for the other CD-1-specific upregulated genes *Mcm4* and *Psma4*), hinting towards a CD-1-strain specific response to infection or associated tissue injury. *Psma4*, a proteasomal subunit (Wang et al., 2015), might fit with this model as well in a paradigm wherein CD-1 mice reinforces cell homeostatic pathways in response to infection or associated tissue injury. More investigation into mechanistically validating the biological significance of a wound healing response during CD-1 infection using parallel avenues of evidence are warranted.

In contrast, B6 Tg inf. mice have a broad adaptive and inflammatory immune response, as discussed by others (Oladunni et al., 2020; Winkler et al., 2020; Yinda et al., 2021). T cell activation, proliferation, and TCR signaling appears uniquely in both GO terms and gene sets for the B6 Tg inf. mice. Most notably, the massively higher number of DEGs and clearly different immune response module is likely heavily driven by the presence of suspected immune infiltrating cells at 2 dpi in the lungs, at the cite of high viral replication and infection. By far the most common GO terms and gene sets are involved in pro-inflammatory pathways. Uniquely, B6 Tg inf. leading edge gene signatures include several chemokines and chemokine receptors genes upregulated relative to WT and non-inf. mice including *Ccl5*, *Ccr5*, *Cxcl16*, and *Ccr2*, hinting towards greater leukocyte infiltration and recruitment especially of monocytes, dendritic cells, and T cells. In support of the presence of immune cells in the B6 Tg inf. lungs, the receptors CCR5 and CCR2 are uniquely present on myeloid cells and monocytes for chemotaxis

(Oppermann, 2004; Tsou et al., 2007; Zeng et al., 2022), respectively, and CXCL16 and CCL5 are produced by dendritic cells, and T cells and monocytes, respectively (Matloubian et al., 2000; Tsou et al., 2007).

In support of the immune cell infiltration model, downregulated during B6 Tg infection include cell-cell structural gene sets associated with adherens junction interactions and laminin interactions that have been demonstrated to sometimes inhibit leukocyte transmigration (Song et al., 2017). An alternative and more likely explanation for this observation is that diseased tissue during infection in the lungs, as demonstrated by others in this B6 Tg inf. model (Oladunni et al., 2020; Winkler et al., 2020; Yinda et al., 2021), have reduced cell-cell structural foundations, as is characteristic during ARDS and acute lung injury, and also seen during fatal COVID-19 (D'Agnillo et al., 2021; Englert et al., 2019; Kása et al., 2015).

The suggested presence of high number of immune infiltrating cells and broader adaptive and inflammatory immune activation is likely driven by higher virus load in these B6 Tg inf. mice compared to the CD-1 KI inf. mice. Indeed, virus load has been shown to influence host response as seen in *in vitro* systems, where greater MOI elicits a broader immune activation, likely due to higher activation of pathogen recognition pathways and downstream innate immunity pathways (pro-inflammatory, interferon, etc.) (Blanco-Melo et al., 2020).

Curiously, B6 Tg inf. mice have decreased compared to non-inf. *Orc4*, a DNA replication initiation factor, *Psmd10*, a proteasomal subunit, and the previously mentioned *Mcm4* as well as downregulated GO terms in developmental pathway of canonical Wnt signaling and RNA transcription. These cell cycle, cell homeostasis, and developmental

downregulation in B6 Tg inf. mice may be due to viral antagonistic effects that are only present at high viral load or due to the broader cell tropism of infection in the B6 Tg inf. mice. Conflicting evidence is presented in the case of enrichment of gene sets in related cell cycle (e.g.: G2/M checkpoints) and DNA replication (e.g.: activation of the pre-replicative complex) pathways. Further investigation is necessary to determine whether cell cycle and DNA replication is indeed up or down during SARS-CoV-2 infection in the B6 Tg mice and what are the biological significances of these findings.

While viral load is clearly higher in B6 Tg inf. mice relative to CD-1 KI inf. mice, the proportion of different viral genomic regions are extremely constant in both infection cases. The similar proportions in the B6 Tg inf. mice, where there is obvious viral replication, can be seen as reassuring proof of active viral replication in the CD-1 KI inf. mice as well (as opposed to the infectious viral titers observed being leftovers from the initial infection inoculum) since proportion of viral genomic regions are crucial to the fitness and reproduction of coronaviruses (Hartenian et al., 2020).

As mentioned previously, *in vitro* studies showed that the level of virus can greatly influence the nature of host response elicited, with a greater interferon and pro-inflammatory response with greater MOI of infection (Blanco-Melo et al., 2020). Using viral reads (CPM) as a substitute for viral abundance, in CD-1 KI inf. mice, significantly positively correlating with viral abundance host genes belong to GO terms associated with T cell signaling. A possible explanation for these uniquely CD-1 KI inf. GO terms may be (1) a more balanced virus level-dependent T cell activation due to lower viral levels (and hence below threshold level for viral protein's antagonistic effects), (2) strain-specific differences, or (3) differential localization of virus or viral antigens for activation of T cells.

Significantly negatively correlating with viral abundance host genes include those belonging to GO terms in the intracellular transport category, indicating disruption of cellular transport network. As a possible explanation, coronaviruses and SARS-CoV-2 disrupt and hijack intracellular transport networks to establish RTC in the ER, to enter the host cell, or to produce new budding virions (Cattin-Ortolá et al., 2021; Hassan et al., 2021; Santerre et al., 2021; Sicari et al., 2020).

Several of these findings mirror observations in human asymptomatic cohorts that were described briefly in the literature review previously. Lower IFN response and ISG expression was noted in asymptomatic human cohorts relative to mild/symptomatic individuals (Wang et al., 2022; Zhang et al., 2021; Zhao et al., 2021), observations also seen in the CD-1 KI infection relative to the B6 Tg infection where there is a broader or higher response despite a few similarities noted. Furthermore, the lower antibody and cell-mediated responses in asymptomatic compared to symptomatic individuals (Long et al., 2020; Mazzoni et al., 2020; Shirin et al., 2020; Zhang et al., 2021) parallels the presence of adaptive immune activation characterized in part by T cell proliferation (e.g.: positive regulation of T cell activation GO term) and APC-lymphocyte (e.g.: immunoregulatory interactions between a lymphoid and a non-lymphoid gene set) signatures in the symptomatic and severe B6 K18-*hACE2* model of SARS-CoV-2 infection compared to the absence of expression and/or enrichment of such genes, GO terms, and gene sets in the asymptomatic CD-1 KI infection model. Furthermore, a recent paper found an overactivation of interferon signaling in critical COVID-19 patients at admission in those with a lethal outcome relative to those with survival outcome (Fava et al., 2022), paralleling the early stronger interferon response (by criteria of broader early

interferon signaling and ISG induction) in the B6 Tg infection relative to the CD-1 KI infection.These preliminary mirroring of host responses is a good starting point to have confidence in the CD-1 KI infection model as a model of asymptomatic COVID-19.

Limitations in this study included the inability to obtain single-cell resolution (in the “bulk RNA-seq” experiment we did, specifically). RNA-seq library preparation also has several limitations (Shi et al., 2021) including fragmentation size bias, and random hexamer and non-specific binding bias however fragment size verification on LabChip GXII instrument and per base sequence content post-trimming with fastqc was used as quality control steps, respectively. RNA-seq also has inherent biases including gene length that can influence the over- and -underrepresentation of a gene’s expression, however, the combination of featureCounts (Liao et al., 2013) and DESeq2’s assumption of a negative binomal distribution minimizes (Love et al., 2014) such effects during differential gene expression analysis. Also, RNA-seq reports only on RNA of course and ignores protein level or post-translationally changes that might occur in both infection models. Complementary approaches looking at proteins and post-translational modifications are warranty.

Second, the smaller sample size (n=3) for the CD-1 KI non-inf. mice, due to 2 samples not passing quality control criteria (low RIN #s, likely due to bad initial RNA quality/RNA degradation because multiple cleaning attempts did not improve quality) for RNA-seq, was an important limitation that underpowers the comparative analysis against CD-1 KI inf. mice and likely results in lower numbers of DEGs, gene expression, GO terms, and gene sets identified due to lower significance in all the aforementioned.

Third, as mentioned previously, the characterization of asymptomatic disease can be done more fully, incorporating functional and histological assessments. In line with these limitations, multiple timepoints throughout the course of infection can be considered to obtain a better viral replication dynamics picture.

Nevertheless, this thesis describes a comprehensive investigation of a novel CD-1 *hACE2* KI model to study SARS-CoV-2 infection and characterizes the host response therein including several unique transcriptomic signatures.

Conclusion and summary

In summary, the CD-1 *hACE2* KI mouse model describes an asymptomatic course of infection characterized by an absence of lethality, no body weight loss, or visual clinical scores despite the presence of infectious viral titers, transcriptomic viral reads, and viral nucleocapsid gene expression. Compared to the severe B6 K18-*hACE2* Tg infection model, there were less DEGs in the CD-1 KI inf. mice. However, in both mouse models, many similarities in gene expression profiles were observed, especially in interferon signaling, interferon-stimulated genes' pathways, and pathogen recognition.

Nevertheless, a unique transcriptomic signature was identified in CD-1 KI inf. mice of decreased coagulation pathways and increased cell cycle & DNA replication, perhaps hinting at a wound healing response that is CD-1-strain specific. In B6 Tg inf. mice, a broader immune activation is observed, likely due to higher immune cell infiltration and recruitment, characterized by increased T cell activation but especially chemokine and cytokine production and signaling.

Finally, viral genomic read proportions were found to be similar in both CD-1 KI inf. and B6 Tg inf. mice, hinting towards active viral replication in the CD-1 KI inf. mice. Viral abundance correlated positively with T cell activation genes in CD-1 KI inf. mice, hinting at a functional T cell response initiation, whereas viral abundance correlated negatively with intracellular transport network genes, indicating viral disruption and hijacking of cellular machinery.

Altogether, a novel asymptomatic mouse model, the CD-1 *hACE2* KI was generated and characterized that may be used for future studies exploring the

determinants of asymptomatic disease or what genetic or environmental perturbations are responsible for transitions to severe disease.

Reference List

Abdelrahman, Z., Li, M., & Wang, X. (2020). Comparative Review of SARS-CoV-2, SARS-CoV, MERS-CoV, and Influenza A Respiratory Viruses [Review]. *Frontiers in Immunology*, *11*. https://doi.org/10.3389/fimmu.2020.552909

Akhtar, A. (2015). The flaws and human harms of animal experimentation. *Cambridge quarterly of healthcare ethics : CQ : the international journal of healthcare ethics committees*, *24*(4), 407-419. https://doi.org/10.1017/S0963180115000079

Alene, M., Yismaw, L., Assemie, M. A., Ketema, D. B., Mengist, B., Kassie, B., & Birhan, T. Y. (2021). Magnitude of asymptomatic COVID-19 cases throughout the course of infection: A systematic review and meta-analysis. *PLOS ONE*, *16*(3), e0249090. https://doi.org/10.1371/journal.pone.0249090

An, H., Hou, J., Zhou, J., Zhao, W., Xu, H., Zheng, Y., Yu, Y., Liu, S., & Cao, X. (2008). Phosphatase SHP-1 promotes TLR- and RIG-I-activated production of type I interferon by inhibiting the kinase IRAK1. *Nat Immunol*, *9*(5), 542-550. https://doi.org/10.1038/ni.1604

Antoniak, S. (2018). The coagulation system in host defense. *Res Pract Thromb Haemost*, *2*(3), 549-557. https://doi.org/10.1002/rth2.12109

Auwaerter, P. M. D. (2022). Coronavirus COVID-19 (SARS-CoV-2). https://www.hopkinsguides.com/hopkins/view/Johns_Hopkins_ABX_Guide/540747/all/Coronavirus_COVID_19__SARS_CoV_2_

Baden, L. R., El Sahly, H. M., Essink, B., Kotloff, K., Frey, S., Novak, R., Diemert, D., Spector, S. A., Rouphael, N., Creech, C. B., McGettigan, J., Khetan, S., Segall, N., Solis, J., Brosz, A., Fierro, C., Schwartz, H., Neuzil, K., Corey, L., . . . Zaks, T. (2021). Efficacy and Safety of the mRNA-1273 SARS-CoV-2 Vaccine. *N Engl J Med*, *384*(5), 403-416. https://doi.org/10.1056/NEJMoa2035389

Bai, Y., Yao, L., Wei, T., Tian, F., Jin, D.-Y., Chen, L., & Wang, M. (2020). Presumed Asymptomatic Carrier Transmission of COVID-19. *JAMA*, *323*(14), 1406-1407. https://doi.org/10.1001/jama.2020.2565

Bastard, P., Rosen, L. B., Zhang, Q., Michailidis, E., Hoffmann, H. H., Zhang, Y., Dorgham, K., Philippot, Q., Rosain, J., Béziat, V., Manry, J., Shaw, E., Haljasmägi, L., Peterson, P., Lorenzo, L., Bizien, L., Trouillet-Assant, S., Dobbs, K., de Jesus, A. A., . . . Casanova, J. L. (2020). Autoantibodies against type I IFNs in patients with life-threatening COVID-19. *Science*, *370*(6515). https://doi.org/10.1126/science.abd4585

Blanco-Melo, D., Nilsson-Payant, B. E., Liu, W. C., Uhl, S., Hoagland, D., Møller, R., Jordan, T. X., Oishi, K., Panis, M., Sachs, D., Wang, T. T., Schwartz, R. E., Lim, J. K., Albrecht, R. A., & tenOever, B. R. (2020). Imbalanced Host Response to SARS-CoV-2 Drives Development of COVID-19. *Cell*, *181*(5), 1036-1045.e1039. https://doi.org/10.1016/j.cell.2020.04.026

Bolger, A. M., Lohse, M., & Usadel, B. (2014). Trimmomatic: a flexible trimmer for Illumina sequence data. *Bioinformatics*, *30*(15), 2114-2120. https://doi.org/10.1093/bioinformatics/btu170

Brant, A. C., Tian, W., Majerciak, V., Yang, W., & Zheng, Z.-M. (2021). SARS-CoV-2: from its discovery to genome structure, transcription, and replication. *Cell & Bioscience*, *11*(1), 136. https://doi.org/10.1186/s13578-021-00643-z

Cattin-Ortolá, J., Welch, L. G., Maslen, S. L., Papa, G., James, L. C., & Munro, S. (2021). Sequences in the cytoplasmic tail of SARS-CoV-2 Spike facilitate expression at the cell surface and syncytia formation. *Nature Communications*, *12*(1), 5333. https://doi.org/10.1038/s41467-021-25589-1

Chen, N., Zhou, M., Dong, X., Qu, J., Gong, F., Han, Y., Qiu, Y., Wang, J., Liu, Y., Wei, Y., Xia, J., Yu, T., Zhang, X., & Zhang, L. (2020). Epidemiological and clinical characteristics of 99 cases of 2019 novel coronavirus pneumonia in Wuhan, China: a descriptive study. *Lancet*, *395*(10223), 507-513. https://doi.org/10.1016/s0140-6736(20)30211-7

Corman, V. M., Muth, D., Niemeyer, D., & Drosten, C. (2018). Hosts and Sources of Endemic Human Coronaviruses. *Advances in virus research*, *100*, 163-188. https://doi.org/10.1016/bs.aivir.2018.01.001

Coronavirus Disease 2019 (COVID-19) Treatment Guidelines. (2021). *National Institutes of Health*. https://www.covid19treatmentguidelines.nih.gov/

Cutler, D. M., & Summers, L. H. (2020). The COVID-19 Pandemic and the $16 Trillion Virus. *JAMA*, *324*(15), 1495-1496. https://doi.org/10.1001/jama.2020.19759

D'Agnillo, F., Walters, K.-A., Xiao, Y., Sheng, Z.-M., Scherler, K., Park, J., Gygli, S., Rosas, L. A., Sadtler, K., Kalish, H., Blatti, C. A., Zhu, R., Gatzke, L., Bushell, C., Memoli, M. J., O'Day, S. J., Fischer, T. D., Hammond, T. C., Lee, R. C., . . . Taubenberger, J. K. (2021). Lung epithelial and endothelial damage, loss of tissue repair, inhibition of fibrinolysis, and cellular senescence in fatal COVID-19. *Science Translational Medicine*, *13*(620), eabj7790. https://doi.org/doi:10.1126/scitranslmed.abj7790

Darif, D., Hammi, I., Kihel, A., El Idrissi Saik, I., Guessous, F., & Akarid, K. (2021). The pro-inflammatory cytokines in COVID-19 pathogenesis: What goes wrong? *Microb Pathog*, *153*, 104799. https://doi.org/10.1016/j.micpath.2021.104799

Das, M., Prasad, S. B., Yadav, S. S., Modi, A., Singh, S., Pradhan, S., & Narayan, G. (2015). HPV-type-specific response of cervical cancer cells to cisplatin after silencing replication licensing factor MCM4. *Tumour Biol*, *36*(12), 9987-9994. https://doi.org/10.1007/s13277-015-3782-7

Deer, R. R., Rock, M. A., Vasilevsky, N., Carmody, L., Rando, H., Anzalone, A. J., Basson, M. D., Bennett, T. D., Bergquist, T., Boudreau, E. A., Bramante, C. T., Byrd, J. B., Callahan, T. J., Chan, L. E., Chu, H., Chute, C. G., Coleman, B. D., Davis, H. E., Gagnier, J., . . . Robinson, P. N. (2021). Characterizing Long COVID: Deep Phenotype of a Complex Condition. *eBioMedicine*, *74*. https://doi.org/10.1016/j.ebiom.2021.103722

Dobin, A., Davis, C. A., Schlesinger, F., Drenkow, J., Zaleski, C., Jha, S., Batut, P., Chaisson, M., & Gingeras, T. R. (2013). STAR: ultrafast universal RNA-seq aligner. *Bioinformatics*, *29*(1), 15-21. https://doi.org/10.1093/bioinformatics/bts635

Englert, J. A., Bobba, C., & Baron, R. M. (2019). Integrating molecular pathogenesis and clinical translation in sepsis-induced acute respiratory distress syndrome. *JCI Insight*, *4*(2). https://doi.org/10.1172/jci.insight.124061

Evans, D. M., & Davey Smith, G. (2015). Mendelian Randomization: New Applications in the Coming Age of Hypothesis-Free Causality. *Annu Rev Genomics Hum Genet*, *16*, 327-350. https://doi.org/10.1146/annurev-genom-090314-050016

Fava, V. M., Bourgey, M., Nawarathna, P. M., Orlova, M., Cassart, P., Vinh, D. C., Cheng, M. P., Bourque, G., Schurr, E., & Langlais, D. (2022). A systems biology approach identifies candidate drugs to reduce mortality in severely ill patients with COVID-19. *Science Advances*, *8*(22), eabm2510. https://doi.org/doi:10.1126/sciadv.abm2510

Finkel, Y., Mizrahi, O., Nachshon, A., Weingarten-Gabbay, S., Morgenstern, D., Yahalom-Ronen, Y., Tamir, H., Achdout, H., Stein, D., Israeli, O., Beth-Din, A., Melamed, S., Weiss, S., Israely, T., Paran, N., Schwartz, M., & Stern-Ginossar, N. (2021). The coding capacity of SARS-CoV-2. *Nature*, *589*(7840), 125-130. https://doi.org/10.1038/s41586-020-2739-1

Fleming, D. S., & Miller, L. C. (2016). Leading edge analysis of transcriptomic changes during pseudorabies virus infection. *Genom Data*, *10*, 104-106. https://doi.org/10.1016/j.gdata.2016.09.014

Frangogiannis, N. G. (2022). Why animal model studies are lost in translation. *J Cardiovasc Aging*, *2*(2). https://doi.org/10.20517/jca.2022.10

Graham, J. B., Swarts, J. L., Leist, S. R., Schäfer, A., Menachery, V. D., Gralinski, L. E., Jeng, S., Miller, D. R., Mooney, M. A., McWeeney, S. K., Ferris, M. T., Pardo-Manuel de Villena, F., Heise, M. T., Baric,

R. S., & Lund, J. M. (2021). Baseline T cell immune phenotypes predict virologic and disease control upon SARS-CoV infection in Collaborative Cross mice. *PLoS Pathog*, *17*(1), e1009287. https://doi.org/10.1371/journal.ppat.1009287

Haddad, F. S. (2004). Ibn Zuhr and experimental tracheostomy and tracheotomy. *Journal of the American College of Surgeons*, *199*(4). https://journals.lww.com/journalacs/Fulltext/2004/10000/Ibn_Zuhr_and_experimental_tracheostomy_and.25.aspx

Hartenian, E., Nandakumar, D., Lari, A., Ly, M., Tucker, J. M., & Glaunsinger, B. A. (2020). The molecular virology of coronaviruses. *J Biol Chem*, *295*(37), 12910-12934. https://doi.org/10.1074/jbc.REV120.013930

Hassan, Z., Kumar, N. D., Reggiori, F., & Khan, G. (2021). How Viruses Hijack and Modify the Secretory Transport Pathway. *Cells*, *10*(10), 2535. https://www.mdpi.com/2073-4409/10/10/2535

Hayashi, A., Ohnishi, H., Okazawa, H., Nakazawa, S., Ikeda, H., Motegi, S., Aoki, N., Kimura, S., Mikuni, M., & Matozaki, T. (2004). Positive regulation of phagocytosis by SIRPbeta and its signaling mechanism in macrophages. *J Biol Chem*, *279*(28), 29450-29460. https://doi.org/10.1074/jbc.M400950200

Holmes, E. C., Goldstein, S. A., Rasmussen, A. L., Robertson, D. L., Crits-Christoph, A., Wertheim, J. O., Anthony, S. J., Barclay, W. S., Boni, M. F., Doherty, P. C., Farrar, J., Geoghegan, J. L., Jiang, X., Leibowitz, J. L., Neil, S. J. D., Skern, T., Weiss, S. R., Worobey, M., Andersen, K. G., . . . Rambaut, A. (2021). The origins of SARS-CoV-2: A critical review. *Cell*, *184*(19), 4848-4856. https://doi.org/10.1016/j.cell.2021.08.017

Huang da, W., Sherman, B. T., & Lempicki, R. A. (2009). Systematic and integrative analysis of large gene lists using DAVID bioinformatics resources. *Nat Protoc*, *4*(1), 44-57. https://doi.org/10.1038/nprot.2008.211

Huff, H. V., & Singh, A. (2020). Asymptomatic Transmission During the Coronavirus Disease 2019 Pandemic and Implications for Public Health Strategies. *Clin Infect Dis*, *71*(10), 2752-2756. https://doi.org/10.1093/cid/ciaa654

Imai, M., Iwatsuki-Horimoto, K., Hatta, M., Loeber, S., Halfmann, P. J., Nakajima, N., Watanabe, T., Ujie, M., Takahashi, K., Ito, M., Yamada, S., Fan, S., Chiba, S., Kuroda, M., Guan, L., Takada, K., Armbrust, T., Balogh, A., Furusawa, Y., . . . Kawaoka, Y. (2020). Syrian hamsters as a small animal model for SARS-CoV-2 infection and countermeasure development. *Proceedings of the National Academy of Sciences*, *117*(28), 16587-16595. https://doi.org/doi:10.1073/pnas.2009799117

Israelow, B., Song, E., Mao, T., Lu, P., Meir, A., Liu, F., Alfajaro, M. M., Wei, J., Dong, H., Homer, R. J., Ring, A., Wilen, C. B., & Iwasaki, A. (2020). Mouse model of SARS-CoV-2 reveals inflammatory role of type I interferon signaling. *Journal of Experimental Medicine*, *217*(12). https://doi.org/10.1084/jem.20201241

Jackson, C. B., Farzan, M., Chen, B., & Choe, H. (2022). Mechanisms of SARS-CoV-2 entry into cells. *Nature Reviews Molecular Cell Biology*, *23*(1), 3-20. https://doi.org/10.1038/s41580-021-00418-x

Jensen, S., & Thomsen, A. R. (2012). Sensing of RNA viruses: a review of innate immune receptors involved in recognizing RNA virus invasion. *Journal of virology*, *86*(6), 2900-2910. https://doi.org/10.1128/JVI.05738-11

Kanwal, Z., Zakrzewska, A., den Hertog, J., Spaink, H. P., Schaaf, M. J. M., & Meijer, A. H. (2013). Deficiency in Hematopoietic Phosphatase Ptpn6/Shp1 Hyperactivates the Innate Immune System and Impairs Control of Bacterial Infections in Zebrafish Embryos. *The Journal of Immunology*, *190*(4), 1631-1645. https://doi.org/10.4049/jimmunol.1200551

Karki, R., Sharma, B. R., Tuladhar, S., Williams, E. P., Zalduondo, L., Samir, P., Zheng, M., Sundaram, B., Banoth, B., Malireddi, R. K. S., Schreiner, P., Neale, G., Vogel, P., Webby, R., Jonsson, C. B., &

Kanneganti, T.-D. (2021). Synergism of TNF-α and IFN-γ Triggers Inflammatory Cell Death, Tissue Damage, and Mortality in SARS-CoV-2 Infection and Cytokine Shock Syndromes. *Cell*, *184*(1), 149-168.e117. https://doi.org/https://doi.org/10.1016/j.cell.2020.11.025

Kása, A., Csortos, C., & Verin, A. D. (2015). Cytoskeletal mechanisms regulating vascular endothelial barrier function in response to acute lung injury. *Tissue Barriers*, *3*(1-2), e974448. https://doi.org/10.4161/21688370.2014.974448

Kopić, A., Benamara, K., Schuster, M., Leidenmühler, P., Bauer, A., Glantschnig, H., & Höllriegl, W. (2019). Coagulation phenotype of wild-type mice on different genetic backgrounds. *Lab Anim*, *53*(1), 43-52. https://doi.org/10.1177/0023677218811059

Korber, B., Fischer, W. M., Gnanakaran, S., Yoon, H., Theiler, J., Abfalterer, W., Hengartner, N., Giorgi, E. E., Bhattacharya, T., Foley, B., Hastie, K. M., Parker, M. D., Partridge, D. G., Evans, C. M., Freeman, T. M., de Silva, T. I., McDanal, C., Perez, L. G., Tang, H., . . . Montefiori, D. C. (2020). Tracking Changes in SARS-CoV-2 Spike: Evidence that D614G Increases Infectivity of the COVID-19 Virus. *Cell*, *182*(4), 812-827.e819. https://doi.org/10.1016/j.cell.2020.06.043

Lahoud, M. H., Proietto, A. I., Gartlan, K. H., Kitsoulis, S., Curtis, J., Wettenhall, J., Sofi, M., Daunt, C., O'Keeffe, M., Caminschi, I., Satterley, K., Rizzitelli, A., Schnorrer, P., Hinohara, A., Yamaguchi, Y., Wu, L., Smyth, G., Handman, E., Shortman, K., & Wright, M. D. (2006). Signal regulatory protein molecules are differentially expressed by CD8- dendritic cells. *J Immunol*, *177*(1), 372-382. https://doi.org/10.4049/jimmunol.177.1.372

Lee, H. K., Knabl, L., Pipperger, L., Volland, A., Furth, P. A., Kang, K., Smith, H. E., Knabl, L., Sr., Bellmann, R., Bernhard, C., Kaiser, N., Gänzer, H., Ströhle, M., Walser, A., von Laer, D., & Hennighausen, L. (2020). Immune transcriptomes of highly exposed SARS-CoV-2 asymptomatic seropositive versus seronegative individuals from the Ischgl community. *medRxiv : the preprint server for health sciences*, 2020.2009.2001.20185884. https://doi.org/10.1101/2020.09.01.20185884

Leist, S. R., Dinnon, K. H., Schäfer, A., Tse, L. V., Okuda, K., Hou, Y. J., West, A., Edwards, C. E., Sanders, W., Fritch, E. J., Gully, K. L., Scobey, T., Brown, A. J., Sheahan, T. P., Moorman, N. J., Boucher, R. C., Gralinski, L. E., Montgomery, S. A., & Baric, R. S. (2020). A Mouse-Adapted SARS-CoV-2 Induces Acute Lung Injury and Mortality in Standard Laboratory Mice. *Cell*, *183*(4), 1070-1085.e1012. https://doi.org/https://doi.org/10.1016/j.cell.2020.09.050

Li, L., Dong, M., & Wang, X. G. (2016). The Implication and Significance of Beta 2 Microglobulin: A Conservative Multifunctional Regulator. *Chin Med J (Engl)*, *129*(4), 448-455. https://doi.org/10.4103/0366-6999.176084

Li, L. L., Wang, J. L., Ma, X. H., Sun, X. M., Li, J. S., Yang, X. F., Shi, W. F., & Duan, Z. J. (2021). A novel SARS-CoV-2 related coronavirus with complex recombination isolated from bats in Yunnan province, China. *Emerg Microbes Infect*, *10*(1), 1683-1690. https://doi.org/10.1080/22221751.2021.1964925

Liao, Y., Smyth, G. K., & Shi, W. (2013). featureCounts: an efficient general purpose program for assigning sequence reads to genomic features. *Bioinformatics*, *30*(7), 923-930. https://doi.org/10.1093/bioinformatics/btt656

Litynski, G. S. (1997). Laparoscopy--the early attempts: spotlighting Georg Kelling and Hans Christian Jacobaeus. *JSLS : Journal of the Society of Laparoendoscopic Surgeons*, *1*(1), 83-85. https://pubmed.ncbi.nlm.nih.gov/9876654

https://www.ncbi.nlm.nih.gov/pmc/articles/PMC3015224/

Long, Q.-X., Tang, X.-J., Shi, Q.-L., Li, Q., Deng, H.-J., Yuan, J., Hu, J.-L., Xu, W., Zhang, Y., Lv, F.-J., Su, K., Zhang, F., Gong, J., Wu, B., Liu, X.-M., Li, J.-J., Qiu, J.-F., Chen, J., & Huang, A.-L. (2020). Clinical and immunological assessment of asymptomatic SARS-CoV-2 infections. *Nature Medicine*, *26*(8), 1200-1204. https://doi.org/10.1038/s41591-020-0965-6

Love, M. I., Huber, W., & Anders, S. (2014). Moderated estimation of fold change and dispersion for RNA-seq data with DESeq2. *Genome Biology*, *15*(12), 550. https://doi.org/10.1186/s13059-014-0550-8

Lu, R., Zhao, X., Li, J., Niu, P., Yang, B., Wu, H., Wang, W., Song, H., Huang, B., Zhu, N., Bi, Y., Ma, X., Zhan, F., Wang, L., Hu, T., Zhou, H., Hu, Z., Zhou, W., Zhao, L., . . . Tan, W. (2020). Genomic characterisation and epidemiology of 2019 novel coronavirus: implications for virus origins and receptor binding. *The Lancet*, *395*(10224), 565-574. https://doi.org/https://doi.org/10.1016/S0140-6736(20)30251-8

Lytras, S., Hughes, J., Martin, D., Swanepoel, P., de Klerk, A., Lourens, R., Kosakovsky Pond, S. L., Xia, W., Jiang, X., & Robertson, D. L. (2022). Exploring the Natural Origins of SARS-CoV-2 in the Light of Recombination. *Genome Biology and Evolution*, *14*(2). https://doi.org/10.1093/gbe/evac018

Ma, Q., Liu, J., Liu, Q., Kang, L., Liu, R., Jing, W., Wu, Y., & Liu, M. (2021). Global Percentage of Asymptomatic SARS-CoV-2 Infections Among the Tested Population and Individuals With Confirmed COVID-19 Diagnosis: A Systematic Review and Meta-analysis. *JAMA Network Open*, *4*(12), e2137257-e2137257. https://doi.org/10.1001/jamanetworkopen.2021.37257

Mahase, E. (2021). Covid-19: Pfizer's paxlovid is 89% effective in patients at risk of serious illness, company reports. *Bmj*, *375*, n2713. https://doi.org/10.1136/bmj.n2713

Mak, I. W., Evaniew, N., & Ghert, M. (2014). Lost in translation: animal models and clinical trials in cancer treatment. *American journal of translational research*, *6*(2), 114-118. https://pubmed.ncbi.nlm.nih.gov/24489990

https://www.ncbi.nlm.nih.gov/pmc/articles/PMC3902221/

Malkova, A., Kudryavtsev, I., Starshinova, A., Kudlay, D., Zinchenko, Y., Glushkova, A., Yablonskiy, P., & Shoenfeld, Y. (2021). Post COVID-19 Syndrome in Patients with Asymptomatic/Mild Form. *Pathogens (Basel, Switzerland)*, *10*(11), 1408. https://doi.org/10.3390/pathogens10111408

Malone, B., Urakova, N., Snijder, E. J., & Campbell, E. A. (2022). Structures and functions of coronavirus replication–transcription complexes and their relevance for SARS-CoV-2 drug design. *Nature Reviews Molecular Cell Biology*, *23*(1), 21-39. https://doi.org/10.1038/s41580-021-00432-z

Mathieu Bourgey, R. D., Robert Eveleigh, Kuang Chung Chen, Louis Letourneau,, Joel Fillon, M. M., Maxime Caron, Johanna Sandoval, Francois Lefebvre,, Gary Leveque, E. M., David Bujold, Pascale Marquis, Patrick Tran Van,, David Morais, J. T., Xiaojian Shao, Edouard Henrion, Emmanuel Gonzalez,, & Pierre-Olivier Quirion, B. C., Guillaume Bourque. (2019). GenPipes: an open-source framework for distributed and scalable genomic analyses. *GigaScience*. https://doi.org/10.1093/gigascience/giz037

Matloubian, M., David, A., Engel, S., Ryan, J. E., & Cyster, J. G. (2000). A transmembrane CXC chemokine is a ligand for HIV-coreceptor Bonzo. *Nature Immunology*, *1*(4), 298-304. https://doi.org/10.1038/79738

Mazzoni, A., Maggi, L., Capone, M., Spinicci, M., Salvati, L., Colao, M. G., Vanni, A., Kiros, S. T., Mencarini, J., Zammarchi, L., Mantengoli, E., Menicacci, L., Caldini, E., Romagnani, S., Liotta, F., Morettini, A., Rossolini, G. M., Bartoloni, A., Cosmi, L., & Annunziato, F. (2020). Cell-mediated and humoral adaptive immune responses to SARS-CoV-2 are lower in asymptomatic than symptomatic COVID-19 patients. *European Journal of Immunology*, *50*(12), 2013-2024. https://doi.org/https://doi.org/10.1002/eji.202048915

McCallum, M., Czudnochowski, N., Rosen, L. E., Zepeda, S. K., Bowen, J. E., Walls, A. C., Hauser, K., Joshi, A., Stewart, C., Dillen, J. R., Powell, A. E., Croll, T. I., Nix, J., Virgin, H. W., Corti, D., Snell, G., & Veesler, D. (2022). Structural basis of SARS-CoV-2 Omicron immune evasion and receptor engagement. *Science*, *375*(6583), 864-868. https://doi.org/10.1126/science.abn8652

Mills, C. D., Kincaid, K., Alt, J. M., Heilman, M. J., & Hill, A. M. (2000). M-1/M-2 macrophages and the Th1/Th2 paradigm. *J Immunol*, *164*(12), 6166-6173. https://doi.org/10.4049/jimmunol.164.12.6166

Mootha, V. K., Lindgren, C. M., Eriksson, K.-F., Subramanian, A., Sihag, S., Lehar, J., Puigserver, P., Carlsson, E., Ridderstråle, M., Laurila, E., Houstis, N., Daly, M. J., Patterson, N., Mesirov, J. P., Golub, T. R., Tamayo, P., Spiegelman, B., Lander, E. S., Hirschhorn, J. N., . . . Groop, L. C. (2003). PGC-1α-responsive genes involved in oxidative phosphorylation are coordinately downregulated in human diabetes. *Nature Genetics*, *34*(3), 267-273. https://doi.org/10.1038/ng1180

Morgan, R. K. (2002). *Altered Carbon*. Victor Gollancz Ltd.

Mukherjee, D., Wagh, G., Mokalled, M. H., Kontarakis, Z., Dickson, A. L., Rayrikar, A., Günther, S., Poss, K. D., Stainier, D. Y. R., & Patra, C. (2021). Ccn2a is an injury-induced matricellular factor that promotes cardiac regeneration in zebrafish. *Development*, *148*(2). https://doi.org/10.1242/dev.193219

Muñoz-Fontela, C., Dowling, W. E., Funnell, S. G. P., Gsell, P.-S., Riveros-Balta, A. X., Albrecht, R. A., Andersen, H., Baric, R. S., Carroll, M. W., Cavaleri, M., Qin, C., Crozier, I., Dallmeier, K., de Waal, L., de Wit, E., Delang, L., Dohm, E., Duprex, W. P., Falzarano, D., . . . Barouch, D. H. (2020). Animal models for COVID-19. *Nature*, *586*(7830), 509-515. https://doi.org/10.1038/s41586-020-2787-6

Neufeldt, C. J., Cerikan, B., Cortese, M., Frankish, J., Lee, J.-Y., Plociennikowska, A., Heigwer, F., Prasad, V., Joecks, S., Burkart, S. S., Zander, D. Y., Subramanian, B., Gimi, R., Padmanabhan, S., Iyer, R., Gendarme, M., El Debs, B., Halama, N., Merle, U., . . . Bartenschlager, R. (2022). SARS-CoV-2 infection induces a pro-inflammatory cytokine response through cGAS-STING and NF-κB. *Communications Biology*, *5*(1), 45. https://doi.org/10.1038/s42003-021-02983-5

Oladunni, F. S., Park, J.-G., Pino, P. A., Gonzalez, O., Akhter, A., Allué-Guardia, A., Olmo-Fontánez, A., Gautam, S., Garcia-Vilanova, A., Ye, C., Chiem, K., Headley, C., Dwivedi, V., Parodi, L. M., Alfson, K. J., Staples, H. M., Schami, A., Garcia, J. I., Whigham, A., . . . Torrelles, J. B. (2020). Lethality of SARS-CoV-2 infection in K18 human angiotensin-converting enzyme 2 transgenic mice. *Nature Communications*, *11*(1), 6122. https://doi.org/10.1038/s41467-020-19891-7

Oppermann, M. (2004). Chemokine receptor CCR5: insights into structure, function, and regulation. *Cell Signal*, *16*(11), 1201-1210. https://doi.org/10.1016/j.cellsig.2004.04.007

Örd, M., Faustova, I., & Loog, M. (2020). The sequence at Spike S1/S2 site enables cleavage by furin and phospho-regulation in SARS-CoV2 but not in SARS-CoV1 or MERS-CoV. *Scientific Reports*, *10*(1), 16944. https://doi.org/10.1038/s41598-020-74101-0

Pairo-Castineira, E., Clohisey, S., Klaric, L., Bretherick, A. D., Rawlik, K., Pasko, D., Walker, S., Parkinson, N., Fourman, M. H., Russell, C. D., Furniss, J., Richmond, A., Gountouna, E., Wrobel, N., Harrison, D., Wang, B., Wu, Y., Meynert, A., Griffiths, F., . . . St George's Hospital, L. U. K. (2021). Genetic mechanisms of critical illness in COVID-19. *Nature*, *591*(7848), 92-98. https://doi.org/10.1038/s41586-020-03065-y

Palacios, E. H., & Weiss, A. (2004). Function of the Src-family kinases, Lck and Fyn, in T-cell development and activation. *Oncogene*, *23*(48), 7990-8000. https://doi.org/10.1038/sj.onc.1208074

Parry, D. A., Tamayo-Orrego, L., Carroll, P., Marsh, J. A., Greene, P., Murina, O., Uggenti, C., Leitch, A., Káposzta, R., Merő, G., Nagy, A., Orlik, B., Kovács-Pászthy, B., Quigley, A. J., Riszter, M., Rankin, J., Reijns, M. A. M., Szakszon, K., & Jackson, A. P. (2020). PRIM1 deficiency causes a distinctive primordial dwarfism syndrome. *Genes Dev*, *34*(21-22), 1520-1533. https://doi.org/10.1101/gad.340190.120

Pertea, M., Pertea, G. M., Antonescu, C. M., Chang, T. C., Mendell, J. T., & Salzberg, S. L. (2015). StringTie enables improved reconstruction of a transcriptome from RNA-seq reads. *Nat Biotechnol*, *33*(3), 290-295. https://doi.org/10.1038/nbt.3122

Planas, D., Saunders, N., Maes, P., Guivel-Benhassine, F., Planchais, C., Buchrieser, J., Bolland, W.-H., Porrot, F., Staropoli, I., Lemoine, F., Péré, H., Veyer, D., Puech, J., Rodary, J., Baela, G., Dellicour, S., Raymenants, J., Gorissen, S., Geenen, C., . . . Schwartz, O. (2021). Considerable escape of SARS-CoV-2 variant Omicron to antibody neutralization. *bioRxiv : the preprint server for biology*, 2021.2012.2014.472630. https://doi.org/10.1101/2021.12.14.472630

Platanias, L. C. (2005). Mechanisms of type-I- and type-II-interferon-mediated signalling. *Nature Reviews Immunology*, *5*(5), 375-386. https://doi.org/10.1038/nri1604

Rambaut, A., Holmes, E. C., O'Toole, Á., Hill, V., McCrone, J. T., Ruis, C., du Plessis, L., & Pybus, O. G. (2020). A dynamic nomenclature proposal for SARS-CoV-2 lineages to assist genomic epidemiology. *Nature Microbiology*, *5*(11), 1403-1407. https://doi.org/10.1038/s41564-020-0770-5

Richard, M., Kok, A., de Meulder, D., Bestebroer, T. M., Lamers, M. M., Okba, N. M. A., Fentener van Vlissingen, M., Rockx, B., Haagmans, B. L., Koopmans, M. P. G., Fouchier, R. A. M., & Herfst, S. (2020). SARS-CoV-2 is transmitted via contact and via the air between ferrets. *Nature Communications*, *11*(1), 3496. https://doi.org/10.1038/s41467-020-17367-2

Robinson, J. T., Thorvaldsdóttir, H., Wenger, A. M., Zehir, A., & Mesirov, J. P. (2017). Variant Review with the Integrative Genomics Viewer. *Cancer Research*, *77*(21), e31-e34. https://doi.org/10.1158/0008-5472.Can-17-0337

Robinson, J. T., Thorvaldsdóttir, H., Winckler, W., Guttman, M., Lander, E. S., Getz, G., & Mesirov, J. P. (2011). Integrative genomics viewer. *Nat Biotechnol*, *29*(1), 24-26. https://doi.org/10.1038/nbt.1754

Robinson, N. B., Krieger, K., Khan, F. M., Huffman, W., Chang, M., Naik, A., Yongle, R., Hameed, I., Krieger, K., Girardi, L. N., & Gaudino, M. (2019). The current state of animal models in research: A review. *International Journal of Surgery*, *72*, 9-13. https://doi.org/https://doi.org/10.1016/j.ijsu.2019.10.015

Rossy, J., Williamson, D. J., & Gaus, K. (2012). How does the kinase Lck phosphorylate the T cell receptor? Spatial organization as a regulatory mechanism. *Front Immunol*, *3*, 167. https://doi.org/10.3389/fimmu.2012.00167

Sabin, A. B. (1965). Oral Poliovirus Vaccine: History of Its Development and Prospects for Eradication of Poliomyelitis. *JAMA*, *194*(8), 872-876. https://doi.org/10.1001/jama.1965.03090210036010

Sanderson, B. (2017). *Oathbringer*. Macmillan.

Santerre, M., Arjona, S. P., Allen, C. N. S., Shcherbik, N., & Sawaya, B. E. (2021). Why do SARS-CoV-2 NSPs rush to the ER? *Journal of Neurology*, *268*(6), 2013-2022. https://doi.org/10.1007/s00415-020-10197-8

Sarkesh, A., Daei Sorkhabi, A., Sheykhsaran, E., Alinezhad, F., Mohammadzadeh, N., Hemmat, N., & Bannazadeh Baghi, H. (2020). Extrapulmonary Clinical Manifestations in COVID-19 Patients. *The American journal of tropical medicine and hygiene*, *103*(5), 1783-1796. https://doi.org/10.4269/ajtmh.20-0986

Schlee, M., & Hartmann, G. (2016). Discriminating self from non-self in nucleic acid sensing. *Nature Reviews Immunology*, *16*(9), 566-580. https://doi.org/10.1038/nri.2016.78

Schneider, W. M., Chevillotte, M. D., & Rice, C. M. (2014). Interferon-stimulated genes: a complex web of host defenses. *Annu Rev Immunol*, *32*, 513-545. https://doi.org/10.1146/annurev-immunol-032713-120231

Schoggins, J. W., & Rice, C. M. (2011). Interferon-stimulated genes and their antiviral effector functions. *Current opinion in virology*, *1*(6), 519-525. https://doi.org/10.1016/j.coviro.2011.10.008

Schubert, K., Karousis, E. D., Jomaa, A., Scaiola, A., Echeverria, B., Gurzeler, L.-A., Leibundgut, M., Thiel, V., Mühlemann, O., & Ban, N. (2020). SARS-CoV-2 Nsp1 binds the ribosomal mRNA channel to

inhibit translation. *Nature Structural & Molecular Biology*, *27*(10), 959-966. https://doi.org/10.1038/s41594-020-0511-8

Sefik, E., Qu, R., Junqueira, C., Kaffe, E., Mirza, H., Zhao, J., Brewer, J. R., Han, A., Steach, H. R., Israelow, B., Blackburn, H. N., Velazquez, S. E., Chen, Y. G., Halene, S., Iwasaki, A., Meffre, E., Nussenzweig, M., Lieberman, J., Wilen, C. B., . . . Flavell, R. A. (2022). Inflammasome activation in infected macrophages drives COVID-19 pathology. *Nature*, *606*(7914), 585-593. https://doi.org/10.1038/s41586-022-04802-1

Sherman, B. T., Hao, M., Qiu, J., Jiao, X., Baseler, M. W., Lane, H. C., Imamichi, T., & Chang, W. (2022). DAVID: a web server for functional enrichment analysis and functional annotation of gene lists (2021 update). *Nucleic Acids Res*. https://doi.org/10.1093/nar/gkac194

Shi, H., Zhou, Y., Jia, E., Pan, M., Bai, Y., & Ge, Q. (2021). Bias in RNA-seq Library Preparation: Current Challenges and Solutions. *BioMed Research International*, *2021*, 6647597. https://doi.org/10.1155/2021/6647597

Shirin, T., Bhuiyan, T. R., Charles, R. C., Amin, S., Bhuiyan, I., Kawser, Z., Rahat, A., Alam, A. N., Sultana, S., Aleem, M. A., Khan, M. H., Khan, S. R., LaRocque, R. C., Calderwood, S. B., Ryan, E. T., Slater, D. M., Banu, S., Clemens, J., Harris, J. B., . . . Qadri, F. (2020). Antibody responses after COVID-19 infection in patients who are mildly symptomatic or asymptomatic in Bangladesh. *International Journal of Infectious Diseases*, *101*, 220-225. https://doi.org/https://doi.org/10.1016/j.ijid.2020.09.1484

Shuai, H., Chan, J. F., Yuen, T. T., Yoon, C., Hu, J. C., Wen, L., Hu, B., Yang, D., Wang, Y., Hou, Y., Huang, X., Chai, Y., Chan, C. C., Poon, V. K., Lu, L., Zhang, R. Q., Chan, W. M., Ip, J. D., Chu, A. W., . . . Chu, H. (2021). Emerging SARS-CoV-2 variants expand species tropism to murines. *eBioMedicine*, *73*, 103643. https://doi.org/10.1016/j.ebiom.2021.103643

Sicari, D., Chatziioannou, A., Koutsandreas, T., Sitia, R., & Chevet, E. (2020). Role of the early secretory pathway in SARS-CoV-2 infection. *Journal of Cell Biology*, *219*(9). https://doi.org/10.1083/jcb.202006005

Singh, D. K., Singh, B., Ganatra, S. R., Gazi, M., Cole, J., Thippeshappa, R., Alfson, K. J., Clemmons, E., Gonzalez, O., Escobedo, R., Lee, T.-H., Chatterjee, A., Goez-Gazi, Y., Sharan, R., Gough, M., Alvarez, C., Blakley, A., Ferdin, J., Bartley, C., . . . Kaushal, D. (2021). Responses to acute infection with SARS-CoV-2 in the lungs of rhesus macaques, baboons and marmosets. *Nature Microbiology*, *6*(1), 73-86. https://doi.org/10.1038/s41564-020-00841-4

Song, E., Zhang, C., Israelow, B., Lu-Culligan, A., Prado, A. V., Skriabine, S., Lu, P., Weizman, O.-E., Liu, F., Dai, Y., Szigeti-Buck, K., Yasumoto, Y., Wang, G., Castaldi, C., Heltke, J., Ng, E., Wheeler, J., Alfajaro, M. M., Levavasseur, E., . . . Iwasaki, A. (2021). Neuroinvasion of SARS-CoV-2 in human and mouse brainNeuroinvasion of SARS-CoV-2 in humans and mice. *Journal of Experimental Medicine*, *218*(3). https://doi.org/10.1084/jem.20202135

Song, J., Zhang, X., Buscher, K., Wang, Y., Wang, H., Di Russo, J., Li, L., Lütke-Enking, S., Zarbock, A., Stadtmann, A., Striewski, P., Wirth, B., Kuzmanov, I., Wiendl, H., Schulte, D., Vestweber, D., & Sorokin, L. (2017). Endothelial Basement Membrane Laminin 511 Contributes to Endothelial Junctional Tightness and Thereby Inhibits Leukocyte Transmigration. *Cell Rep*, *18*(5), 1256-1269. https://doi.org/10.1016/j.celrep.2016.12.092

Subramanian, A., Tamayo, P., Mootha Vamsi, K., Mukherjee, S., Ebert Benjamin, L., Gillette Michael, A., Paulovich, A., Pomeroy Scott, L., Golub Todd, R., Lander Eric, S., & Mesirov Jill, P. (2005). Gene set enrichment analysis: A knowledge-based approach for interpreting genome-wide expression profiles. *Proceedings of the National Academy of Sciences*, *102*(43), 15545-15550. https://doi.org/10.1073/pnas.0506580102

Subramanian, A., Tamayo, P., Mootha, V. K., Mukherjee, S., Ebert, B. L., Gillette, M. A., Paulovich, A., Pomeroy, S. L., Golub, T. R., Lander, E. S., & Mesirov, J. P. (2005). Gene set enrichment analysis:

A knowledge-based approach for interpreting genome-wide expression profiles. *Proceedings of the National Academy of Sciences*, *102*(43), 15545-15550. https://doi.org/doi:10.1073/pnas.0506580102

Sun, J., Zhuang, Z., Zheng, J., Li, K., Wong, R. L., Liu, D., Huang, J., He, J., Zhu, A., Zhao, J., Li, X., Xi, Y., Chen, R., Alshukairi, A. N., Chen, Z., Zhang, Z., Chen, C., Huang, X., Li, F., . . . Zhao, J. (2020). Generation of a Broadly Useful Model for COVID-19 Pathogenesis, Vaccination, and Treatment. *Cell*, *182*(3), 734-743.e735. https://doi.org/10.1016/j.cell.2020.06.010

Sun, S. H., Chen, Q., Gu, H. J., Yang, G., Wang, Y. X., Huang, X. Y., Liu, S. S., Zhang, N. N., Li, X. F., Xiong, R., Guo, Y., Deng, Y. Q., Huang, W. J., Liu, Q., Liu, Q. M., Shen, Y. L., Zhou, Y., Yang, X., Zhao, T. Y., . . . Wang, Y. C. (2020). A Mouse Model of SARS-CoV-2 Infection and Pathogenesis. *Cell Host Microbe*, *28*(1), 124-133.e124. https://doi.org/10.1016/j.chom.2020.05.020

Sureshchandra, S., Zulu, M. Z., Doratt, B. M., Jankeel, A., Tifrea, D., Edwards, R., Rincon, M., Marshall, N. E., & Messaoudi, I. (2022). Single-cell RNA sequencing reveals immunological rewiring at the maternal-fetal interface following asymptomatic/mild SARS-CoV-2 infection. *Cell Reports*, *39*(11). https://doi.org/10.1016/j.celrep.2022.110938

Tahir, M. (2021). Coronavirus genomic nsp14-ExoN, structure, role, mechanism, and potential application as a drug target. *J Med Virol*, *93*(7), 4258-4264. https://doi.org/10.1002/jmv.27009

Tang, D., Kang, R., Coyne, C. B., Zeh, H. J., & Lotze, M. T. (2012). PAMPs and DAMPs: signal 0s that spur autophagy and immunity. *Immunol Rev*, *249*(1), 158-175. https://doi.org/10.1111/j.1600-065X.2012.01146.x

Thorvaldsdóttir, H., Robinson, J. T., & Mesirov, J. P. (2012). Integrative Genomics Viewer (IGV): high-performance genomics data visualization and exploration. *Briefings in Bioinformatics*, *14*(2), 178-192. https://doi.org/10.1093/bib/bbs017

Threadgill, D. W., Miller, D. R., Churchill, G. A., & de Villena, F. P. (2011). The collaborative cross: a recombinant inbred mouse population for the systems genetic era. *Ilar j*, *52*(1), 24-31. https://doi.org/10.1093/ilar.52.1.24

Timmermans, S. (2003). A Black Technician and Blue Babies. *Social Studies of Science*, *33*(2), 197-229. https://doi.org/10.1177/03063127030332014

Tsou, C. L., Peters, W., Si, Y., Slaymaker, S., Aslanian, A. M., Weisberg, S. P., Mack, M., & Charo, I. F. (2007). Critical roles for CCR2 and MCP-3 in monocyte mobilization from bone marrow and recruitment to inflammatory sites. *J Clin Invest*, *117*(4), 902-909. https://doi.org/10.1172/jci29919

V'kovski, P., Kratzel, A., Steiner, S., Stalder, H., & Thiel, V. (2021). Coronavirus biology and replication: implications for SARS-CoV-2. *Nature Reviews Microbiology*, *19*(3), 155-170. https://doi.org/10.1038/s41579-020-00468-6

Van Dam, D., & De Deyn, P. P. (2011). Animal models in the drug discovery pipeline for Alzheimer's disease. *British journal of pharmacology*, *164*(4), 1285-1300. https://doi.org/10.1111/j.1476-5381.2011.01299.x

van Kessel, S. A. M., Olde Hartman, T. C., Lucassen, P. L. B. J., & van Jaarsveld, C. H. M. (2022). Post-acute and long-COVID-19 symptoms in patients with mild diseases: a systematic review. *Family practice*, *39*(1), 159-167. https://doi.org/10.1093/fampra/cmab076

Wang, H., Li, X., Li, T., Zhang, S., Wang, L., Wu, X., & Liu, J. (2020). The genetic sequence, origin, and diagnosis of SARS-CoV-2. *European journal of clinical microbiology & infectious diseases : official publication of the European Society of Clinical Microbiology*, *39*(9), 1629-1635. https://doi.org/10.1007/s10096-020-03899-4

Wang, T., Chen, T., Thakur, A., Liang, Y., Gao, L., Zhang, S., Tian, Y., Jin, T., Liu, J. J., & Chen, M. (2015). Association of PSMA4 polymorphisms with lung cancer susceptibility and response to cisplatin-

based chemotherapy in a Chinese Han population. *Clin Transl Oncol*, *17*(7), 564-569. https://doi.org/10.1007/s12094-015-1279-x

Wang, X., Bai, H., Ma, J., Qin, H., Zeng, Q., Hu, F., Jiang, T., Mao, W., Zhao, Y., Chen, X., Qi, X., Li, M., Xu, J., Hao, J., Wang, Y., Ding, X., Liu, Y., Huang, T., Fang, C., . . . Zhang, C. (2022). Identification of Distinct Immune Cell Subsets Associated With Asymptomatic Infection, Disease Severity, and Viral Persistence in COVID-19 Patients [Original Research]. *Frontiers in Immunology*, *13*. https://doi.org/10.3389/fimmu.2022.812514

Wendler, A., & Wehling, M. (2010). The translatability of animal models for clinical development: biomarkers and disease models. *Curr Opin Pharmacol*, *10*(5), 601-606. https://doi.org/10.1016/j.coph.2010.05.009

Winkler, E. S., Bailey, A. L., Kafai, N. M., Nair, S., McCune, B. T., Yu, J., Fox, J. M., Chen, R. E., Earnest, J. T., Keeler, S. P., Ritter, J. H., Kang, L. I., Dort, S., Robichaud, A., Head, R., Holtzman, M. J., & Diamond, M. S. (2020). SARS-CoV-2 infection of human ACE2-transgenic mice causes severe lung inflammation and impaired function. *Nat Immunol*, *21*(11), 1327-1335. https://doi.org/10.1038/s41590-020-0778-2

Wirasinha, R. C., Davies, A. R., Srivastava, M., Sheridan, J. M., Sng, X. Y. X., Delmonte, O. M., Dobbs, K., Loh, K. L., Miosge, L. A., Lee, C. E., Chand, R., Chan, A., Yap, J. Y., Keller, M. D., Chen, K., Rossjohn, J., La Gruta, N. L., Vinuesa, C. G., Reid, H. H., . . . Daley, S. R. (2021). Nfkb2 variants reveal a p100-degradation threshold that defines autoimmune susceptibility. *J Exp Med*, *218*(2). https://doi.org/10.1084/jem.20200476

Wolff, G., Melia, C. E., Snijder, E. J., & Bárcena, M. (2020). Double-Membrane Vesicles as Platforms for Viral Replication. *Trends in Microbiology*, *28*(12), 1022-1033. https://doi.org/10.1016/j.tim.2020.05.009

Woolsey, C., Borisevich, V., Prasad, A. N., Agans, K. N., Deer, D. J., Dobias, N. S., Heymann, J. C., Foster, S. L., Levine, C. B., Medina, L., Melody, K., Geisbert, J. B., Fenton, K. A., Geisbert, T. W., & Cross, R. W. (2021). Establishment of an African green monkey model for COVID-19 and protection against re-infection. *Nature Immunology*, *22*(1), 86-98. https://doi.org/10.1038/s41590-020-00835-8

World Health Organization. (2020). *WHO Director-General's opening remarks at the media briefing on COVID-19 - 11 March 2020*

Retrieved 25/09/2021 from https://www.who.int/director-general/speeches/detail/who-director-general-s-opening-remarks-at-the-media-briefing-on-covid-19---11-march-2020

Yan, W., Zheng, Y., Zeng, X., He, B., & Cheng, W. (2022). Structural biology of SARS-CoV-2: open the door for novel therapies. *Signal Transduction and Targeted Therapy*, *7*(1), 26. https://doi.org/10.1038/s41392-022-00884-5

Yinda, C. K., Port, J. R., Bushmaker, T., Offei Owusu, I., Purushotham, J. N., Avanzato, V. A., Fischer, R. J., Schulz, J. E., Holbrook, M. G., Hebner, M. J., Rosenke, R., Thomas, T., Marzi, A., Best, S. M., de Wit, E., Shaia, C., van Doremalen, N., & Munster, V. J. (2021). K18-hACE2 mice develop respiratory disease resembling severe COVID-19. *PLoS Pathog*, *17*(1), e1009195. https://doi.org/10.1371/journal.ppat.1009195

You, Y., Yang, X., Hung, D., Yang, Q., Wu, T., & Deng, M. (2021). Asymptomatic COVID-19 infection: diagnosis, transmission, population characteristics. *BMJ Supportive & Palliative Care*, bmjspcare-2020-002813. https://doi.org/10.1136/bmjspcare-2020-002813

Zeng, Z., Lan, T., Wei, Y., & Wei, X. (2022). CCL5/CCR5 axis in human diseases and related treatments. *Genes & Diseases*, *9*(1), 12-27. https://doi.org/https://doi.org/10.1016/j.gendis.2021.08.004

Zhang, J., Lin, D., Li, K., Ding, X., Li, L., Liu, Y., Liu, D., Lin, J., Teng, X., Li, Y., Liu, M., Shen, J., Wang, X., He, D., Shi, Y., Wang, D., & Xu, J. (2021). Transcriptome Analysis of Peripheral Blood Mononuclear

Cells Reveals Distinct Immune Response in Asymptomatic and Re-Detectable Positive COVID-19 Patients [Original Research]. *Frontiers in Immunology*, *12*. https://doi.org/10.3389/fimmu.2021.716075

Zhang, L., Li, Q., Liang, Z., Li, T., Liu, S., Cui, Q., Nie, J., Wu, Q., Qu, X., Huang, W., & Wang, Y. (2022). The significant immune escape of pseudotyped SARS-CoV-2 variant Omicron. *Emerg Microbes Infect*, *11*(1), 1-5. https://doi.org/10.1080/22221751.2021.2017757

Zhang, Q., Bastard, P., Liu, Z., Le Pen, J., Moncada-Velez, M., Chen, J., Ogishi, M., Sabli Ira, K. D., Hodeib, S., Korol, C., Rosain, J., Bilguvar, K., Ye, J., Bolze, A., Bigio, B., Yang, R., Arias Andrés, A., Zhou, Q., Zhang, Y., . . . Zhang, X. (2020). Inborn errors of type I IFN immunity in patients with life-threatening COVID-19. *Science*, *370*(6515), eabd4570. https://doi.org/10.1126/science.abd4570

Zhao, X.-N., You, Y., Cui, X.-M., Gao, H.-X., Wang, G.-L., Zhang, S.-B., Yao, L., Duan, L.-J., Zhu, K.-L., Wang, Y.-L., Li, L., Lu, J.-H., Wang, H.-B., Fan, J.-F., Zheng, H.-W., Dai, E.-H., Tian, L.-Y., & Ma, M.-J. (2021). Single-cell immune profiling reveals distinct immune response in asymptomatic COVID-19 patients. *Signal Transduction and Targeted Therapy*, *6*(1), 342. https://doi.org/10.1038/s41392-021-00753-7

Zhou, H., Ji, J., Chen, X., Bi, Y., Li, J., Wang, Q., Hu, T., Song, H., Zhao, R., Chen, Y., Cui, M., Zhang, Y., Hughes, A. C., Holmes, E. C., & Shi, W. (2021). Identification of novel bat coronaviruses sheds light on the evolutionary origins of SARS-CoV-2 and related viruses. *Cell*, *184*(17), 4380-4391.e4314. https://doi.org/10.1016/j.cell.2021.06.008

Zhou, S., Butler-Laporte, G., Nakanishi, T., Morrison, D. R., Afilalo, J., Afilalo, M., Laurent, L., Pietzner, M., Kerrison, N., Zhao, K., Brunet-Ratnasingham, E., Henry, D., Kimchi, N., Afrasiabi, Z., Rezk, N., Bouab, M., Petitjean, L., Guzman, C., Xue, X., . . . Richards, J. B. (2021). A Neanderthal OAS1 isoform protects individuals of European ancestry against COVID-19 susceptibility and severity. *Nature Medicine*, *27*(4), 659-667. https://doi.org/10.1038/s41591-021-01281-1

Zou, L., Ruan, F., Huang, M., Liang, L., Huang, H., Hong, Z., Yu, J., Kang, M., Song, Y., Xia, J., Guo, Q., Song, T., He, J., Yen, H.-L., Peiris, M., & Wu, J. (2020). SARS-CoV-2 Viral Load in Upper Respiratory Specimens of Infected Patients. *New England Journal of Medicine*, *382*(12), 1177-1179. https://doi.org/10.1056/NEJMc2001737